MAPPING OF ANNUAL ICE LAYER EXTENT AND SNOW ACCUMULATION IN THE PERCOLATION ZONE OF THE GREENLAND ICE SHEET: QUICKSCAT APPLICATION AND GREENLAND CLIMATE NETWORK

Konrad Steffen, Russell Huff, and Jose Rial*

University of Colorado at Boulder
Cooperative Institute for Research in Environmental Sciences
Campus Box 216, Boulder CO 80309
*Visiting Faculty Fellow at CIRES

NASA Grant NNG06GB08G

Progress Report
to
National Aeronautics and Space Administration
December 2006

With contributions by Manfred Stober, Sabrina Baur, and Stefan Reinhart
Stuttgart University of Applied Sciences, Department of Surveying and Geoinformatics.

ICE FJORD IN NORTHWEST GREENLAND CLOSE TO QAANAAQ

TABLE OF CONTENTS

1. Field Expedition 2006

1.1 Logistic Summary

Date	Location	Work
April 2006		
25	Scotia-SFJ	Team members (Steffen, Huff) and cargo on C-130
25	CPH-SFJ	Team members (Frei, Kaser) with Air Greenland
26	SFJ-NASA U	AWS maintenance and download
26	NASA U – Qaanaaq	Overnight
27	Qaanaaq – NEEM	New AWS install, future deep drilling site (EU-NSF)
27	NEEM – GITS – Qaa.	No landing at GITS AWS, overnight
28	Qaa. – Thule – HUM	Pick-up Rignot at Thule, Humboldt AWS maintenance
28	HUM – Qaanaaq	Overnight
29	Qaa. – Pet ELA – Qaa.	Petermann ELA AWS maintenance
May 2006		
1	Qaa. - Petermann	Petermann Glacier AWS maintenance, R. Huff accident
1	Petermann – Thule AFB	R. Huff to Thule AFB hospital, overnight
2	Thule – Summit	Summit AWS maintenance, overnight
3	Summit – NASA E – Summit	NASA E AWS maintenance, overnight
4	Summit – SFJ	End of northern AWS maintenance tour
4	SFJ	E.Rignot and G. Kaser leaving
6	SFJ – SC - SFC	Cargo flight to Swiss Camp
7	SFJ – Dye-2 – Saddle SFJ	AWS maintenance at Dye-2 and Saddle
6	Scotia – SFJ	Team members arrive (Zwally, Rial, Sampson, Koenig)
6	CPH – SFJ	Team member Frei arrives with AirGreenland
8	SFJ – SC	Put-in (Steffen, Zwally, Sampson, Rial, Frei, Koenig)
10	SC region	JAR1, 2; SMS1, 2, 3 visit with skidoo, data download
13	SC region	JAR1 AWS maintenance and re-drilling
14	Ilulissat – SC	Media visit (Haeusler/FACTS and Bannet/Nat. Geog)
17	Ilulissat – SC	H.J Frei and K. Schroff arrive, wind turbine installation
22	SC – SFJ	H.J. Frei and Schroff leave
23	SC region	Installation of 2 new GPS and AWS with Twin Otter
23	SC – SFJ	Close of Swiss Camp and leaving to Kangerlussuaq

SFJ: Sonderstromfjord/Kangerlussuaq
SC: Swiss Camp

1.2 Automatic Weather Station Maintenance

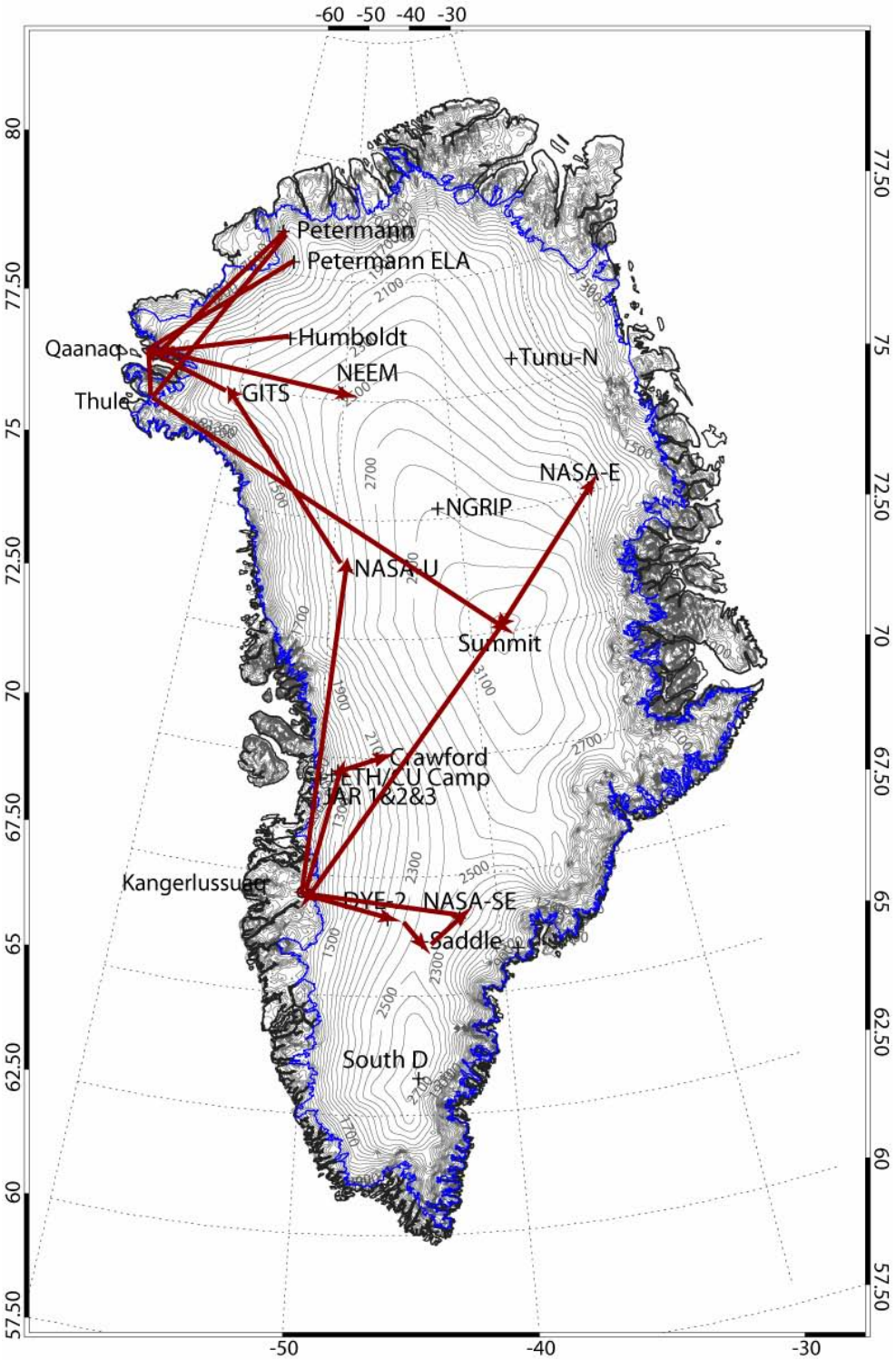

Figure 1.1: Greenland Climate Network (GC-Net) automatic weather stations as of summer 2006. The red arrows indicate the Twin Otter flight path for the AWS maintenance described in the logistic summary.

1.3 Personal

Name	Institution	Arr.	Dep.
AWS support and Swiss Camp research			
Konrad Steffen	CU-Boulder	4/25	5/26
Russ Huff	CU-Boulder	4/25	5/1
Georg Kaser	Uni. Innsbruck	4/25	5/8
Eric Rignot	NASA-JPL	4/28	5/4
Kevin Sampson	CU-Boulder	5/7	5/26
Jay Zwally	NASA-GSFC	5/7	5/26
Jose Rial	Univ. North Carolina	5/7	5/26
Lora Koenig	Univ. Washington	5/7	5/26
Louis Frei	ETH Switzerland	5/7	5/26
Karl Schroff	ETH Switzerland	5/17	5/22
HansJuerg Frei	ETH Switzerland	5/17	5/22
Moulin Experiment			
Konrad Steffen	CU-Boulder	8/14	8/19
Alberto Behar	NASA-JPL	8/14	8/19

2. Greenland Climate Network (GC-Net)

2.1 Overview

The GC-Net currently consists of 19 automatic weather stations and four smart stakes distributed over the entire Greenland ice sheet (Figure 1.1). Four stations are located along the crest of the ice sheet (2500 to 3200 m elevation range) in a north-south direction, Eight stations are located close to the 2000 m contour line (1830 m to 2500 m), and four stations are positioned in the ablation region (50 m to 800 m), and two stations are located at the equilibrium line altitude at the west coast and in the north.). The smart stakes were introduced in spring 2001 to measure the climate in the ablation region in the Jakobshavn area (SMS1-4), and one on the floating tongue of Petermann Gletscher.

The GC-Net was established in spring 1995 with the intention of monitoring climatological and glaciological parameters at various locations on the ice sheet over a time period of at least 10 years. The first AWS was installed in 1990 at the Swiss Camp, followed by four AWS in 1995, four in 1996, five in 1997, another four in 1999, one in 2002 and the latest one in 2003. Our objectives for the Greenland weather station (AWS) network are to measure daily, annual and interannual variability in accumulation rate, surface climatology and surface energy balance at selected locations on the ice sheet, and to measure near-surface snow density at the AWS locations for the assessment of snow densification, accumulation, and metamorphosis.

In addition to providing climatological and glaciological observations from the field, further application of the GC-Net data include: the study of the ice sheet melt extent [*Abdalati and Steffen*, 2001]; estimates of the ice sheet sublimation rate [*Box and Steffen*, 2001]; reconstruction of long-term air temperature time series [*Shuman at al.*, 2001], assessment of surface climate [*Steffen and Box*, 2001], and the interpretation of satellite-derived melt features of the ice sheet [*Nghiem et al.*, 2001]. Potential applications for the use of the GC-Net data are: comparison of in-situ and satellite-derived surface parameters, operational weather forecast; validation of climate models; and logistic support for ice camps and Thule AFB.

2.2 GC-Net Users

During the last 12 month we received 50 GC-Net data request and distributed the data using the new Web interface. This web interface allows us to capture the email and affiliation of all GC-Net users, including a short description of their use of the Greenland Climate data. The data request is processed on a UNIX 4-processor workstation and the data is transferred on a FTP site for direct downloading. We will continue top maintain the main portal for all GC-Net data distribution, the main radon being the frequent data reprocessing to increase data quality.

In the following the latest 32 users of GC-Net data are listed by email, name and affiliation since June, 2006. They all used the web-based interface (given below) to request the Greenland climate data for model validation, process studies, satellite comparison, and more.

Home page of GC-Net and web interface for data request:
http://cires.colorado.edu/science/groups/steffen/gcnet/

Greenland Climate Network Data Request

ID	Email	Name	Organization
108	jemitchell@mail.ecsu.edu	Jerome Mitchell	UNH
109	gcatania@utig.ig.utexas.edu	Ginny Catania	University of Texas
110	me@toddalbert.com	Todd Albert	Florida State University
111	krinner@ujf-grenoble.fr	Gerhard Krinner	LGGE/CNRS
112	Christo-pher.A.Shuman@nasa.gov	Christopher Shuman	NASA Goddard Space Flight Center
113	mmccabe@lanl.gov	Matthew McCabe	Los Alamos National Laboratory
114	ehanna@sheffield.ac.uk	Edward Hanna	University of Sheffield
115	djl22@psu.edu	Derrick J Lampkin	Department of Geography, Pennsylvania State University
117	vtsai@fas.harvard.edu	Victor Tsai	Harvard University
120	chylek@lanl.gov	Petr Chylek	Los Alamos National Laboratory
121	chylek@lanl.gov	Petr Chylek	LANL
122	marc.simard@jpl.nasa.gov	Marc Simard	JPL
123	marc.simard@jpl.nasa.gov	Marc Simard	JPL
124	dorothy.k.hall@nasa.gov	Dorothy Hall	NASA GSFC Code 614.1
125	dorothy.k.hall@nasa.gov	Dorothy K. Hall	NASA GSFC Code 614.1
126	ashuler@ldeo.columbia.edu	Ashley Shuler	Columbia University
127	ashuler@ldeo.columbia.edu	Ashley Shuler	Lamont Doherty Earth Observatory
128	mtedesco@umbc.edu	Marco Tedesco	UMBC/NASA
129	patrickspiers@gmail.com	Patrick Spiers	Icebird expedition and NSW Dept. of Education and Training.
130	patrickspiers@gmail.com	Patrick Spiers	icebird expedition and NSW Dept. of Education and Training.
131	fain@lgge.obs.ujf-grenoble.fr	fain	Laboratoire de Glaciologie et Géophysique de l'Environnement
132	maurerj@nsidc.org	John Maurer	National Snow and Ice Data Center
133	mtedesco@umbc.edu	Marco Tedesco	NASA/UMBC
134	li.li@nrl.navy.mil	Li Li	Naval Research Laboratory
135	0303523t@student.gla.ac.uk	Carolyn Thomson	University of Glasgow
136	ursula.rick@colorado.edu	Ursula Rick	INSTAAR
137	louisedavid-son0302@hotmail.com	louise davidson	student
138	nicola.delcore@libero.it	Nicola	Infocenter
139	tejsrejs@yahoo.dk	Tejs Møller	Høgskulen i Volda, Norway
140	Madeleinewiles@hotmail.co.uk	Madeleine Wiles	Edinburgh University

2.3 GC-Net Citation List

This list represents publications that made use of Greenland Climate Network (GC-Net) data.

Abdalati, W. and K. Steffen, Greenland ice sheet melt extent: 1979-1999, *J. Geophys. Res*., 106(D24), 33,983-33,989, 2001.

Box, J.E., D.H. Bromwich1, B.A. Veenhuis, Le-S. Bai, J.C. Stroeve, J.C. Rogers, K. Steffen, T. Haran, S.-H.. Wang, Greenland ice sheet surface mass balance variability (1988-2004) from calibrated Polar MM5 output, *J.Clim.*, 2005.

Box, J. E., Surface Water Vapor Exchange on the Greenland Ice Sheet Derived from Automated Weather Station Data, PhD Thesis, Department of Geography, University of Colorado, Boulder, CO, Cooperative Institute for Research in Environmental Sciences, 190 pp, 2001.

Box, J.E. and K. Steffen, Sublimation on the Greenland ice sheet from automated weather station observations, *J. Geophys. Res*., 106(D24), 33,965-33,982, 2001.

Bromwhich, D., J. Cassano, T. Klein, G. Heinemann, K. Hines, K. Steffen and J. Box, Mesoscale modeling of katabatic winds over Greenland with Polar MM5, *Mon. Weather Review*, 129, 2290-2309, 2001.

Cassano, J.J., J.E. Box, D.H. Bromwich, L. Li, and K. Steffen, Evaluation of Polar MM5 simulations of Greenland's atmospheric circulation, *J. Geophys. Res*., 106(D24), 33,867-33,890, 2001.

Cullen, N., and K. Steffen, Unstable near-surface boundary conditions in summer on top of the Greenland ice sheet., *Geophys. Res. Lett*., 28(23), 4491-4494, 2001.

Davis, C.H. and D.M. Segura, An algorithm for time-series analysis of ice sheet surface elevations from satellite altimetry, *IEEE Transactions on Geoscience & Remote Sensing*, 39(1), 202-206, 2001.

Dassau, T.M., A. Sumer, S. Koeniger, P. Shepson, J. Yang, R. Honrath, N. Culen, K. Steffen, Investigation of the role of the snowpack on atmospheric formaldehyde chemistry at Summit, Greenland, J. Geophys. Res., 107(D19), ACH 9.1-14, 36, 2595-2608, 2002.

Hanna,H., P.Huybrechts, I. Janssens, J..Cappelen, K. Steffen, and A. Stephens, Runoff and mass balance of the Greenland ice sheet: 1958–2003, *J. Geophys. Res.*, 110, D13108, doi:10.1029/2004JD005641, 2005.

Hanna, E. and P. Valdes, Validation of ECMWF (re)analysis surface climate data, 1979-1998, for Greenland and implications for mass balance modeling of the Ice Sheet, *Intern. J. Clim.*, 21, 171-195, 2001.

Helmig, D, J. Boulter, D. David, J. Birk, N. Cullen, K. Steffen, B. Johsnon, S. Oltmans, Ozone and meteorological boundary-layer conditions at Summit, Greenland, *Atm. Environm*., 36, 2595-2608, 2002.

Honrath, R.E. Y.Y. Lu, M.C. Peterson, J.E. Dibb, M.A. Arseault, N.J. Cullen, and K. Steffen. vertical fluxes of NOx, HONO, and HNO3 above the snowpack at Summit, Greenland. *Atm. Environm*, 36, 2629-2640, 2002.

Klein, T., G. Heinemann, D. H. Bromwich, J. J. Cassano and K. M. Hines, Mesoscale modeling of katabatic winds over Greenland and comparisons with AWS and aircraft data, *J. Met. Atmos. Phys*., 8(1/2), 115-132, 2001.

Klein, T., G. Heinemann, Simulations of the katabatic wind over the Greenland ice sheet with a 3D model for one winter month and two spring months, Report of the DAAD/NSF project 315-PP, 1999.

Mosley-Thompson, E., J.R. McConnell, R.C. Bales, Z. Li, P.-N. Lin, K. Steffen, L.G. Thompson, R. Edwards, D. Bathke, Local to regional-scale variability of annual net accumulation on the Greenland ice sheet from PARCA cores, *J. Geophys. Res*., 106 (D24), 33,839-33852, 2001.

Murphy, B. F., I. Marsiat and P. Valdes, Simulated atmospheric contributions to the surface mass balance of Greenland. *J. Geophys. Res.*, 106, submitted, 2001.

Nghiem,S,V., K. Steffen, G. Neumann, and R. Huff, Mapping of ice layer extent and snow accumulation in the percolation zone of the Greenland ice sheet, *J. Geophys., Res*., 110, F02017, doi:10.1029/2004JF000234, 2005.

Nghiem, S.V., K. Steffen, R. Kwok, and W.Y. Tsai, Diurnal variations of melt regions on the Greenland ice sheet, *J. Glaciol*., 47(159), 539-547, 2001.

Nolin, A. and J. Stroeve The Changing Albedo of the Greenland Ice Sheet: Implications for Climate Change, Annals of Glaciology, 25, 51-57, 1997.

Orr, A., E. Hanna, J. Hunt, J. Cappelen, K. Steffen and A. Stephens, Characteristics of stable flow over southern Greenland, *Pure and Applied Geophysics (PAGEOPH)*, 161(7), 2004.

Serreze, M., J. Key, J. Box, J. Maslanik, and K. Steffen, A new monthly climatology of global radiation for the Arctic and comparison with NCEP-NCAR reanalysis and ISCCP-C2 field, *J. Climate*, 11, 121-136, 1998.

Shuman, C., K. Steffen, J. Box, and C. Stearn, A dozen years of temperature observations at the Summit: Central Greenland automatic weather stations 1987-1999, *J. Appl. Meteorol*., 40(4),741-752, 2001.

Smith, L.C., Y. Sheng, R.R. Foster, K. Steffen, K.E. Frey, and D.E. Alsdorf, Melting of small Arctic ice caps observed from ERS scatterometer time series, Geophys. Res. Lett., 30(20), CRY 2-14, 2003.

Steffen, K., S.V. Nghiem, R. Huff, and G. Neumann, The melt anomaly of 2002 on the Greenland Ice Sheet from active and passive microwave satellite observations, *Geophys. Res. Lett., 31*(20), L2040210.1029/2004GL020444, 2004.

Steffen, K., and J.E. Box, Surface climatology of the Greenland ice sheet: Greenland climate network 1995-1999, *J. Geophys. Res*., 106(D24), 33,951-33,964, 2001.

Steffen, K., W. Abdalati, and I. Serjal, Hoar development on the Greenland ice sheet, *J. of Glaciology*, 45(148), 63-68, 1999.

Steffen, K., J. E. Box and W. Abdalati, Greenland climate network: GC-Net, *CRREL, 98-103* pp., 1996.

Stroeve, J., Assessment of Greenland Albedo Variability from the AVHRR Polar Pathfinder Data Set, *J. Geophys. Res*., 106(D24), 33,989-34,006, 2001.

Stroeve, J., and A. Nolin, 1997. The changing albedo of the Greenland ice sheet: implications for climate modeling, *Ann. of Glaciol*., 25, 51-57.

Stroeve, J, J. E. Box, J. Maslanik, J. Key, C. Fowler, Intercomparison between in situ and AVHRR Polar Pathfinder-derived surface albedo over Greenland, *Remote Sensing of the Environment*, 75(3), 360-374, 2001.

Thomas, R., and PARCA instigators, Program for Arctic Regional Climate Assessment (PARCA): Goals, key findings, and future directions, *J. Geophys. Res.*, 106(D24), 33,691-33706, 2001.

Thomas, R.H., W. Abdalati, E. Frederick, W.B. Krabill, S. Manizade, and K. Steffen, Investigation of surface melting and dynamic thinning on Jakobshavn Isbrea, Greenland, J. Glaciol., 49(165), 231-239, 2003.

Zwally, H.J. W. Abdalati, T. Herring, K. Larsen, J. Saba, and K. Steffen. Surface melt-induced acceleration of Greenland ice-sheet flow, *Science*, 297, 218-222, 2002.

3. Results

3.1 Melt Climatology

3.1.1 Melt detection enhancement and validation using GC-Net

Comparison of the passive microwave based XPGR melt detection algorithm with GC-Net temperature records and QSCAT underscores some of the strengths and weaknesses of the XPGR. When aggregated annually the active microwave identifies 20% more melt days than the passive. The length of the passive microwave melt record (27 years) and conservative nature of the melt detection algorithm are the primary advantages of the XPGR for annually averaged melt studies. The AM detects surficial levels of melt, higher in the percolation zone and in the northwest. The PM detects longer melt duration in the southeast and the west where melt is more intense with deeper snow packs. The primary weakness of the XPGR is a tendency to underestimate melt on bare ice surfaces. An improved melt detection algorithm was developed by applying lapse rates developed using the GC-Net data (*Steffen and Box*, 2001). This analysis resulted in two major byproducts, namely an estimate of the melting bare ice area (Fig. 3.1.1) as well as an estimate of the positive degree days for the past 27 years. The amount of melting bare ice has increased at an astonishing rate of 13% per year (99% significant). These results indicate that melt is dominating the surface mass balance of the ice sheet in the lower ablation region in spite of modeled and observed increases in precipitation (*Box et al.*, 2006; *Nghiem et al.*, 2005).

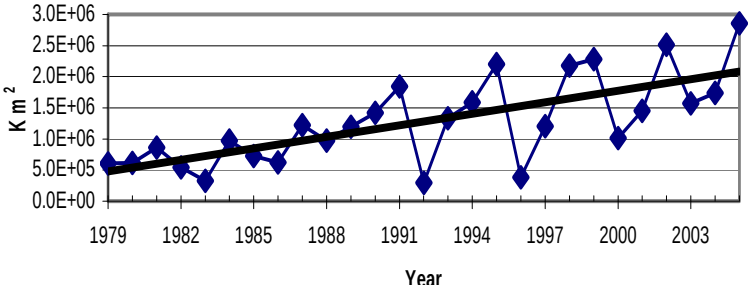

Figure 3.1.1 The total amount of melting bare ice accounted for using the lapse rate enhanced passive microwave melt detection method.

3.1.2 Melt variability

The annual melt signal since 1979 is highly variable with a standard deviation that is 28% of the mean (Fig. 3.1.2). Error bars on the annual total melt area are computed for the first time based on the GC-Net air temperature record. The total melt area in Greenland has increased at a rate of 1.4% per year since 1979 (91% significant.) The melt signal is highly periodic repeating every 3 or 4 years. The record melt year occurred in 2005 but the five maximum years on record are within 11% of the 2005 record. The 1992 melt year, following the Mt. Pinatubo eruption, is the minimum melt year on record at 2 standard deviations below the mean followed closely by 1996 (1.6 standard deviations below the mean.) Peak melt occurs, on average, on August 1st. Increasing trends during July (1.7% per year, 90% significant) and August (1.9% per year, 95% significant) are largely responsible for the overall annual trend (Fig. 3.1.3). The onset and duration of the melt season have not changed significantly. The largest increases in melt have occurred in the north (3.2% per year, 95% significant, Fig. 3.1.4) and the west (1.8% per year, 98% significant, Fig. 3.1.5). The melt trend on the east side of the ice sheet is not statistically significant (Fig. 3.1.6). The lowest probability melt event occurred in 2002 when prolonged melt occurred in the

northeast above 1000m elevation. Low probability melt events resulting from above average melt have increased significantly (95%) since 1979.

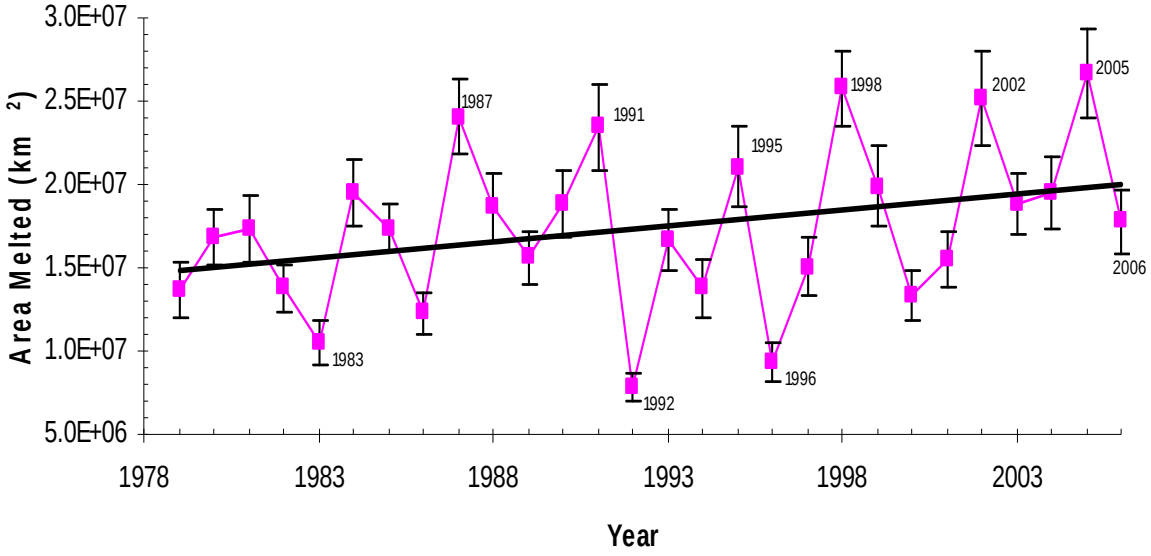

Figure 3.1.2 Total area experiencing melt during each annual melt cycle summed from April 1 through October 31. Error bars represent the 95% confidence interval.

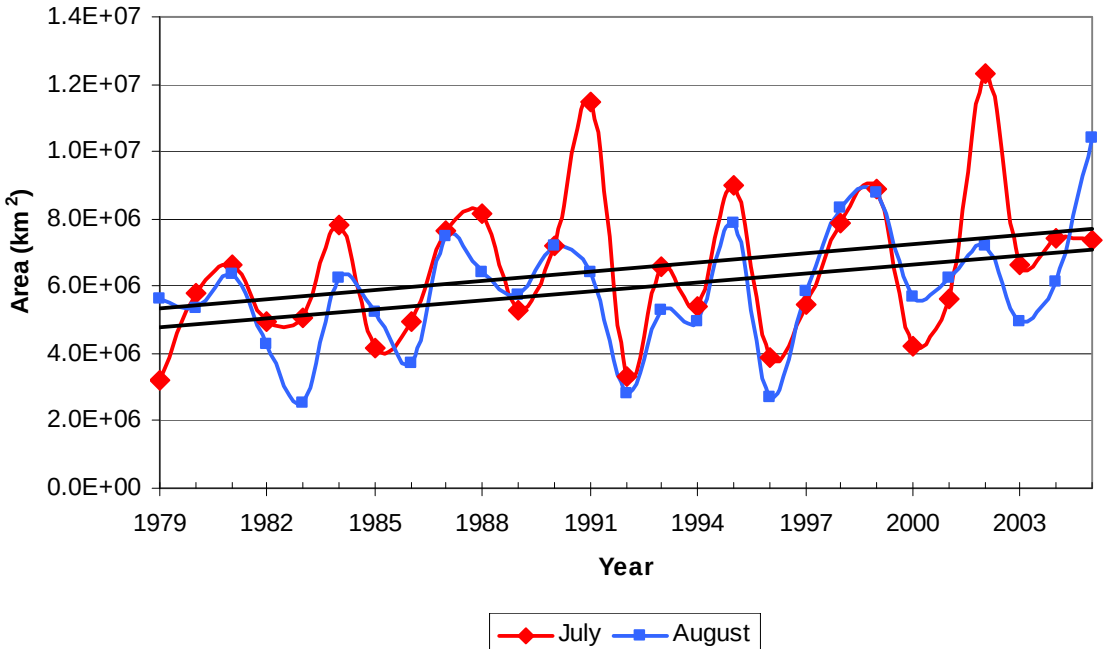

Figure 3.1.3 Total melt area for July and August. The trend in July is significant at the 0.90 level and in August the trend is significant at the 0.95 level.

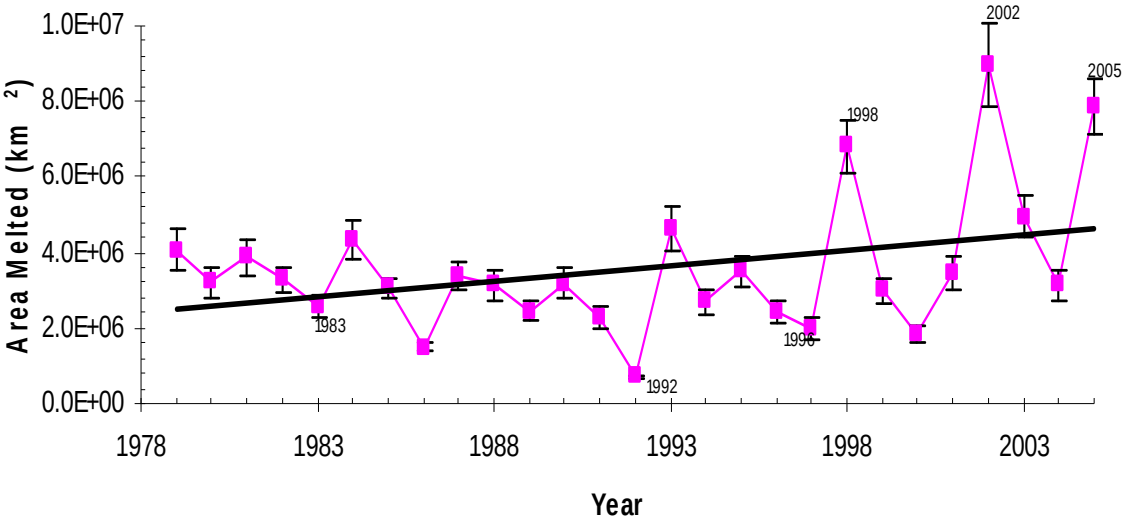

Figure 3.1.4 Total melt area for northern Greenland from 1979-2005. Error bars are for the 95% confidence interval. The trend is significant (94%).

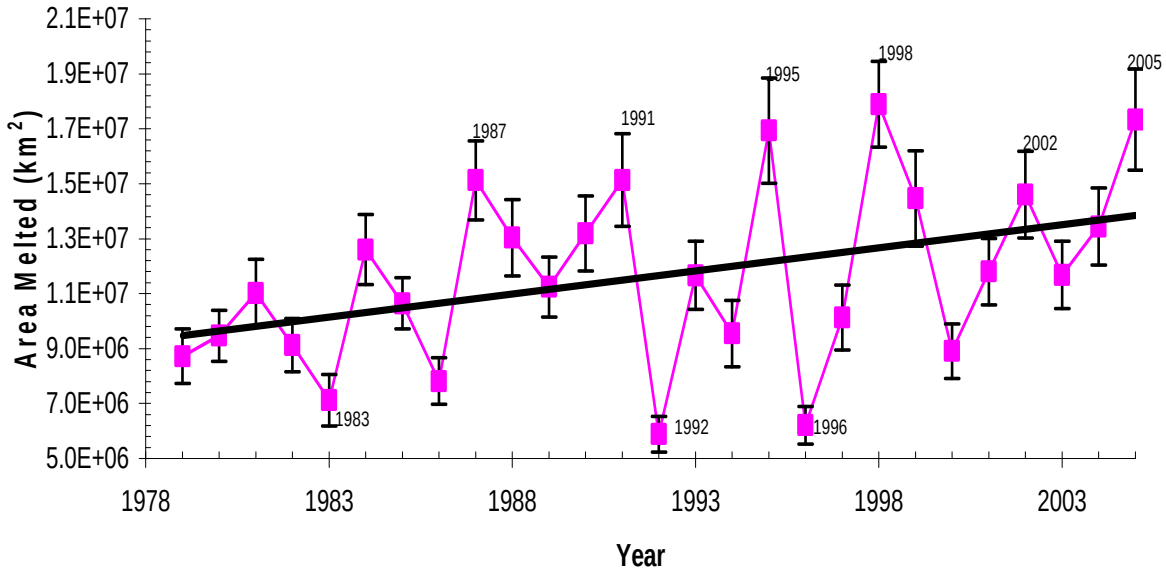

Figure 3.1.5 Total annual melt area for the west side of the Greenland ice sheet. Error bars are based on the 95% confidence interval for each annual value. The trend is significant (95%).

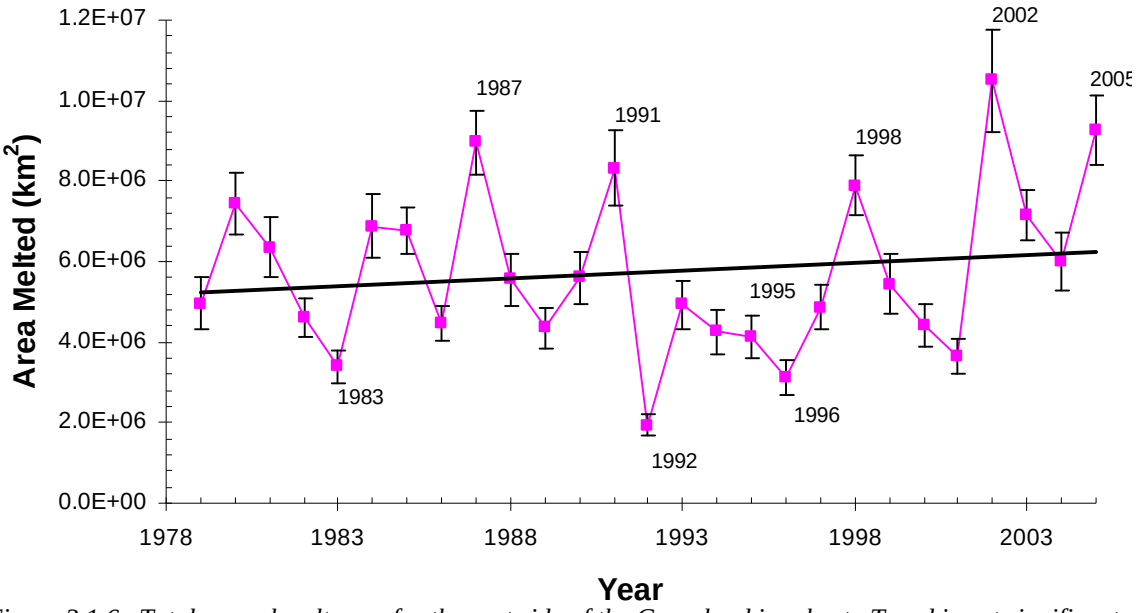

Figure 3.1.6. Total annual melt area for the east side of the Greenland ice sheet. Trend is not significant.

3.1.3 Passive linking melt anomalies and large scale atmospheric circulation

Relationships between melt variability in Greenland and changes in large scale circulation patterns are identified by first correlating the melt signal with the pressure and the SAT signals. This identifies circulation patterns that are coincident in time with the melt pattern. The NAO, during winter in particular, is a well known pattern of atmospheric circulation that influences climate in the north Atlantic. It is therefore reasonable to expect variability in the NAO to influence melt in Greenland although much of the research associated with the NAO has focused on the winter. The melt signal in Greenland is compared with the NAO both in terms of the NAO index and the SLP patterns associated with both signals using regression analysis and compositing extreme years.

The mean (April-September) geopotential heights related to above or below average melt years can be computed by regressing the melt signal onto the 750 hPa geopotential height field. During below average melt years there is a low pressure trough over the central Arctic that extends symmetrically over Greenland (see the 2925m, black contour, Fig. 3.1.7) Air flow over Greenland is predominately from the north. As melt increases from below to above average, the low pressure trough fills and rotates to the west (compare the 2900m contours, Fig. 3.1.7). Average heights to the southeast of Greenland increase from 2910m to 2950m. The implied geostrophic flow onto Greenland during peak melt years now has a more southerly component. Since the melt signal is very cyclical, the low pressure trough is swinging back and forth across Greenland every three to four years.

The seasonal mean geopotential height field averages synoptic scale conditions. Therefore, Figure 3.1.7 implies that during maximum melt years there are more cyclones passing along the west coast of Greenland and relatively few to the east. Cyclones west of Greenland will pull warmer, moist air from the south. Cyclones east of Greenland will generally entrain cooler northeasterly flow onto the ice sheet. The increasing melt trends in western and northwestern Greenland imply that, on average, atmospheric conditions favoring southerly flow increasingly dominate. These

observations are corroborated by the SAT anomalies associated with melt in Greenland (Fig. 3.1.8).

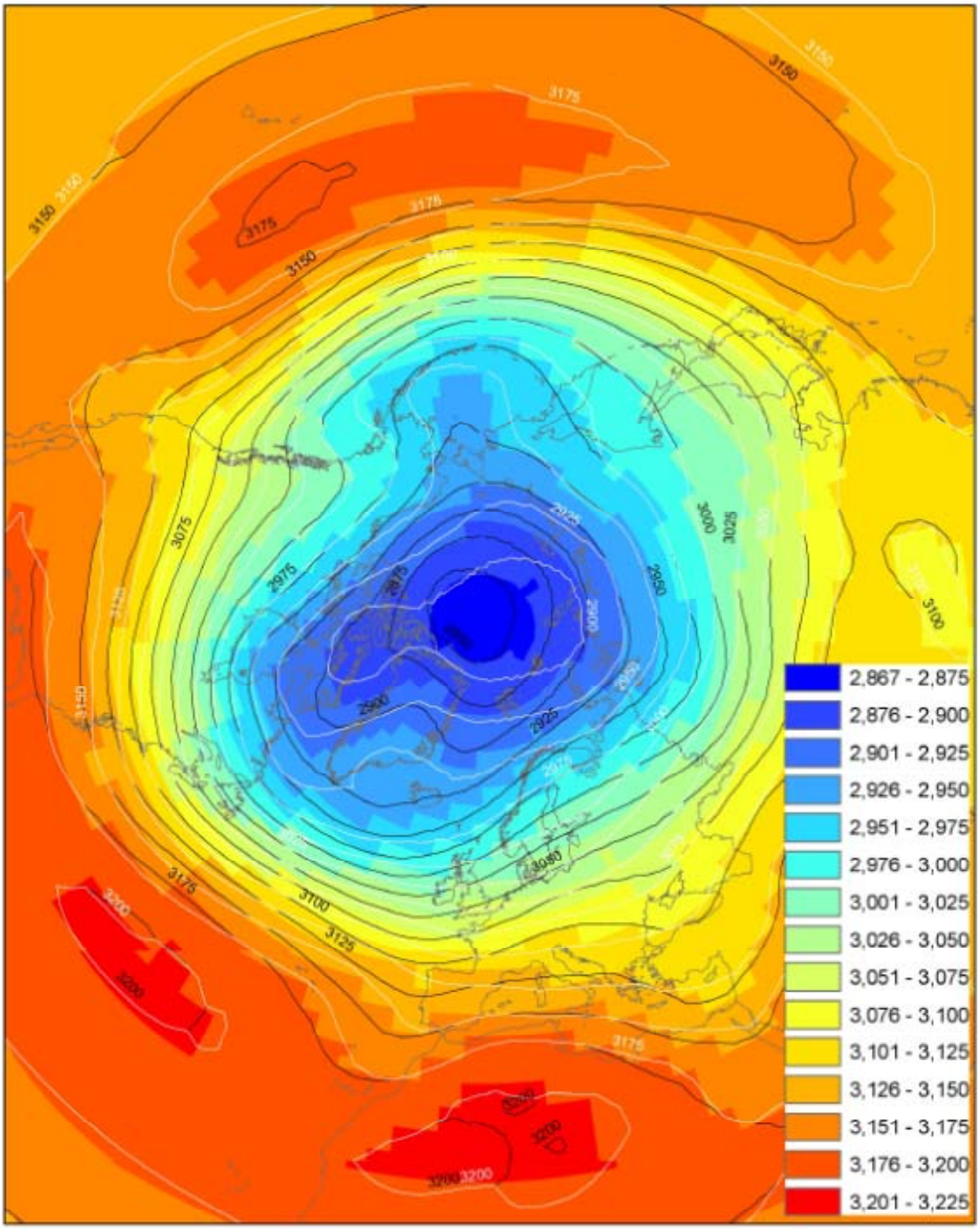

Figure 3.1.7 The 750 hPa geopotential height field associated with a -2 standard deviation melt year (black contours) and a +2 standard deviation melt year (white contours). Shading is the mean 750 hPa geopotential height field for 1979-2003. Units are meters.

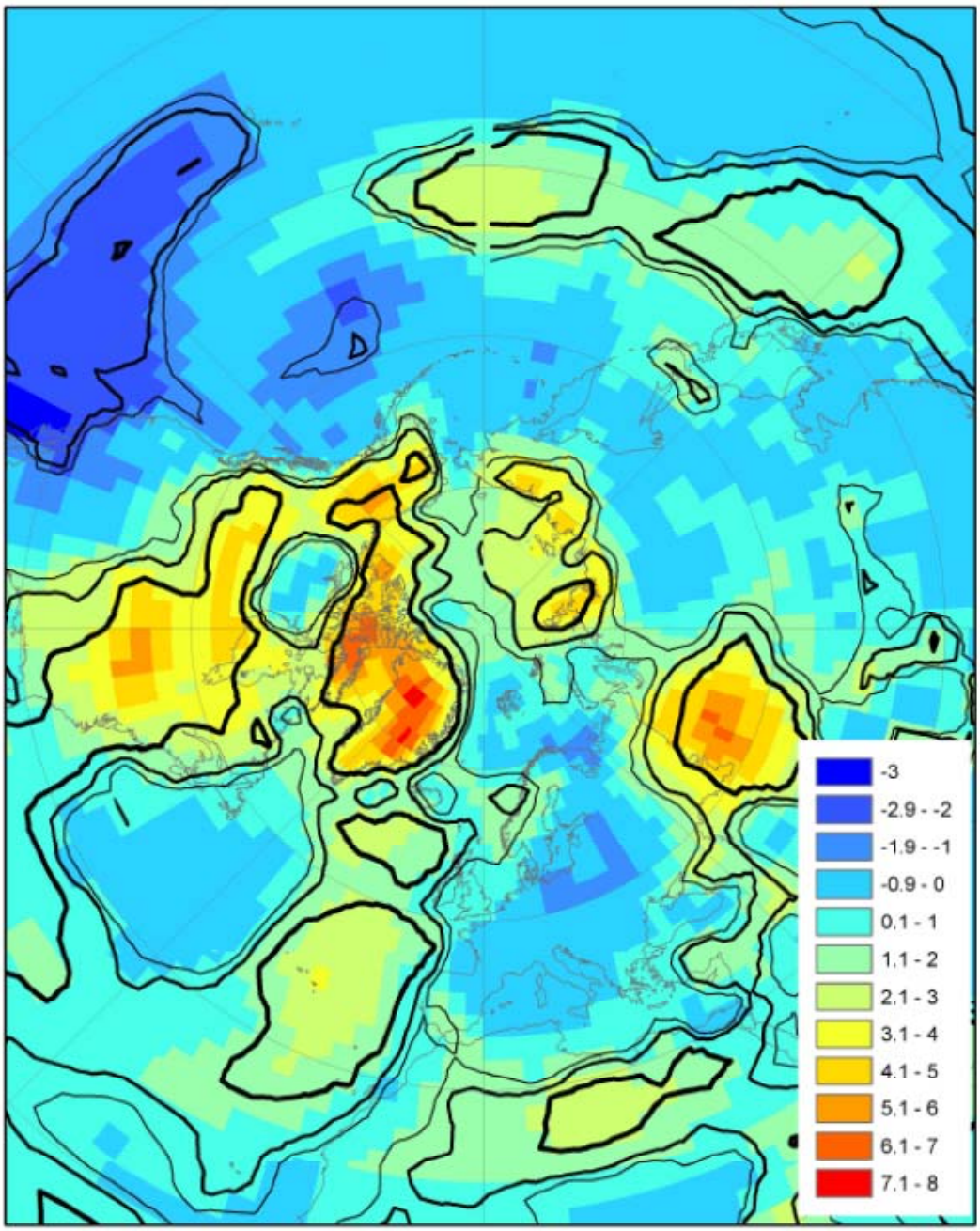

Figure 3.1.8 Melt season (May-September) SAT anomalies associated with the leading melt EOF. The pattern was constructed by linearly regressing the SAT anomalies onto the melt PC1. The field is in units of tenths of degrees C per standard deviation of the melt PC. Contours are the 99%, 95% and 90% significance levels (thick, medium, thin line, respectively).

As the trough over Greenland swings from east to west and melt progresses from minimum to maximum, the Aleutian Low deepens (see the 2950 contours, Fig. 3.1.7) while the Pacific High intensifies (see the 3175 contours, Fig. 3.1.7). A pattern emerges indicative of a cyclical redistribution of low pressure from the east to the west of the Arctic. This introduces a possible connection between melt in Greenland and conditions in the North Pacific.

The spatial pattern of SLP anomalies associated with the NAO and the melt signal are broadly similar but display several key differences. First, the SLP anomalies associated with the NAO are not confined to east of Greenland but extend to both sides of the ice sheet. Secondly, the NAO related anomalies do not display a center of action over west central Canada. In other words, the NAO related pressure anomalies do not reflect the see-saw from east to west of Greenland that drives the melt variability. Similarly, the NAO index (June-July) and the melt signal are 45% correlated (Fig. 3.1.9) indicative of a linkage between the two phenomena since 1979. However, prior to 2000, the two signals are correlated at 57%. If the melt years influenced by the Mt. Pinatubo eruption are removed (1992, 1993, 1994) the NAO and the melt signal are 76% correlated through 1999. Since 1999 the correlation between the melt signal and the NAO index has reversed sign. What happened in 1999? A possible explanation is that the Pacific component, not captured by the NAO, has played a stronger role since 1999. Prior to 2000 the melt signal is not correlated with the PNA (10%). However, since 1999 the two signals are correlated at 96% although the number of samples is too small to be conclusive.

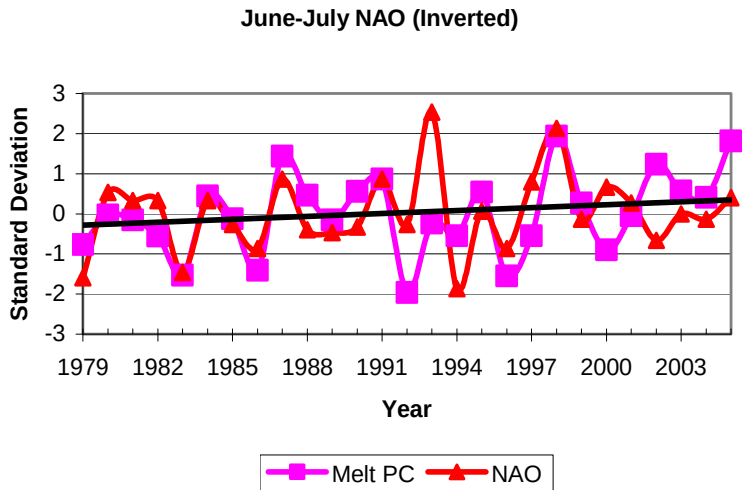

Figure 3.1.9 Standardized teleconnection indices (inverted) for the NAO relative to the melt PC1.

Variability in the spatial distribution of sea ice in the Arctic, and the Canadian Arctic in particular, is correlated with melt variability in Greenland (Fig. 3.1.10). The major areas of sea ice variability in the Canadian Arctic include the east and west coasts of Greenland, Hudson Bay and the Beaufort Sea. These regions coincide with SLP anomalies related to melt. Southwesterly flow into Greenland is enhanced during peak melt years which likely decreases sea ice concentrations in the Hudson Bay and Baffin Bay. Similarly, the positive pressure anomalies east of the Beaufort Sea coupled with negative pressure anomalies over Alaska, (which are associated with enhanced melt in Greenland), likely result in decreased sea ice concentrations in the Beaufort Sea. Sea ice concentration anomalies northeast of Greenland are generally of opposite sign to those of southwest Greenland. This observation further indicates that the sea ice anomalies in the vicinity of Greenland are related to the same warm-season circulation patterns responsible for melt variability on the ice sheet.

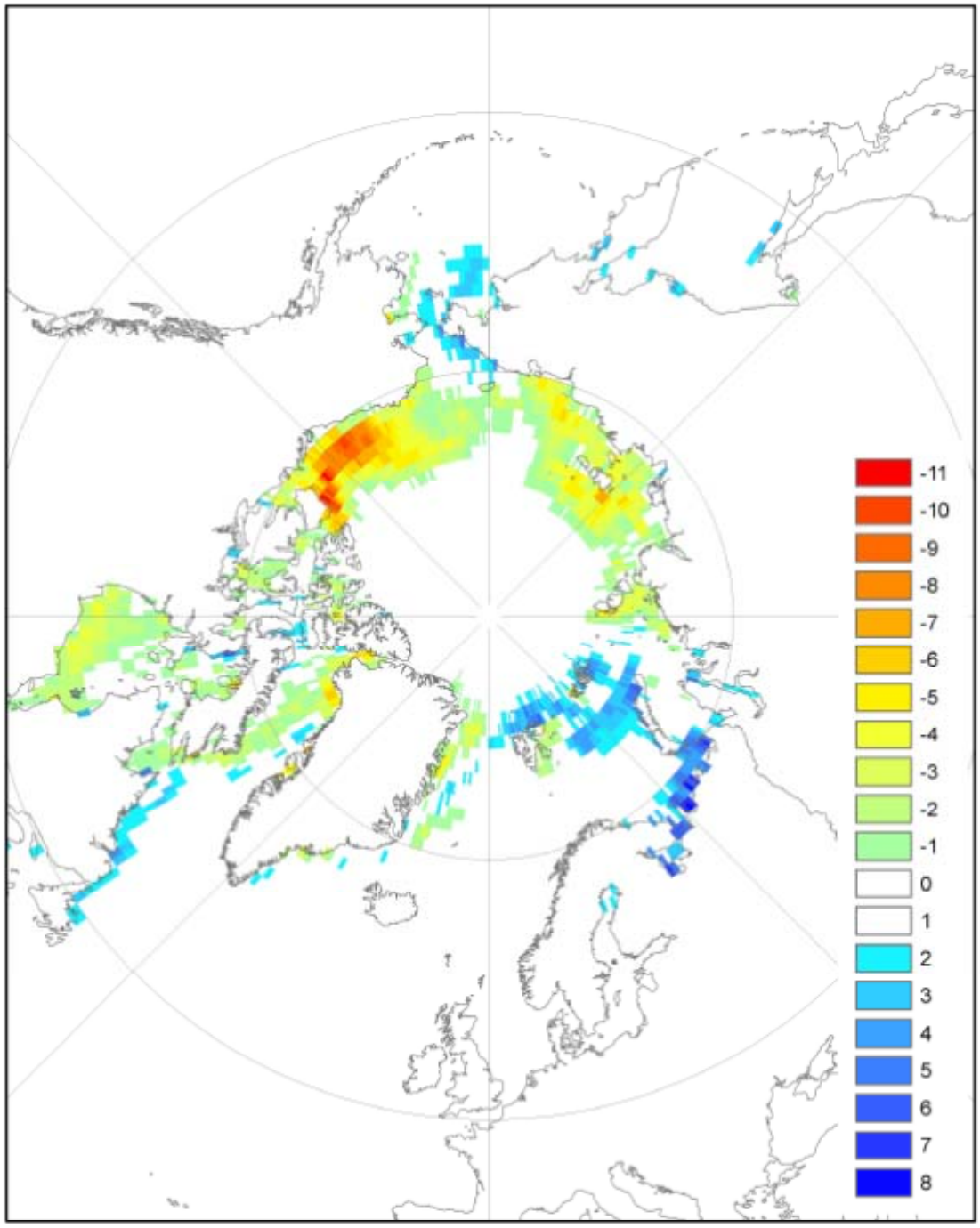

Figure 3.1.10 Melt season (May-September) sea ice anomalies associated with the leading melt EOF. The pattern was constructed by linearly regressing the sea ice anomalies onto the melt PC1. The field is in units of % concentration per standard deviation of the melt PC.

3.2 Seismic Monitoring of Greenland's Ice Sheet (SMOGIS)

3.2.1 The seismic deployment

With the collaboration of researchers from the University of Colorado and starting funding from CIRES (U. Colorado, Boulder), instrument support by NSF and logistic support by NASA, we have begun the seismic monitoring of Greenland's ice sheet in the neighborhood of Swiss Camp, a meteorological/glaciological permanent station operated by Dr. Konrad Steffen (U. of Colorado, Boulder) since the spring of 1990.

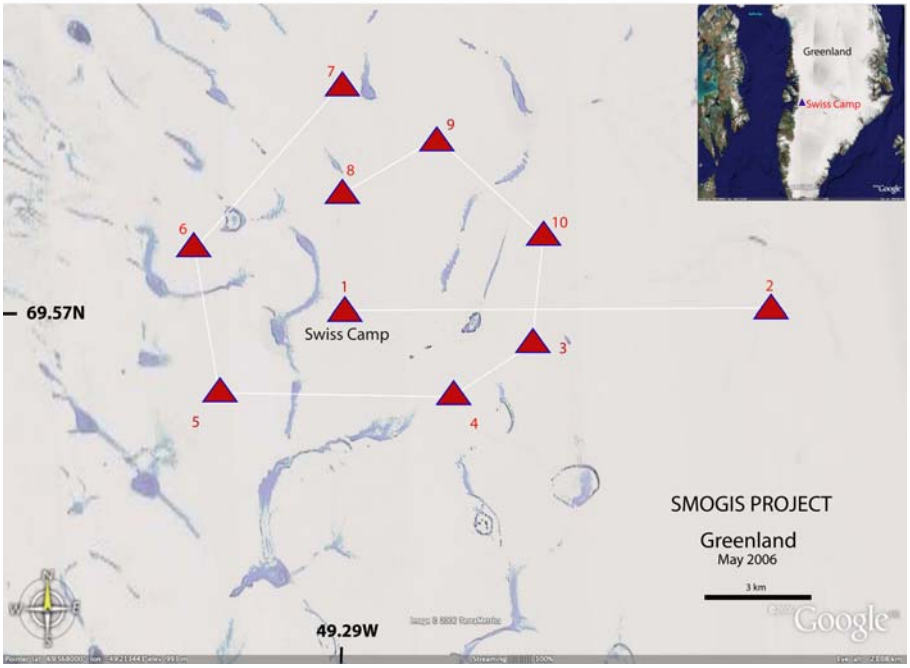

Figure 3.2.1 The portable seismic array deployed in the neighborhood of Swiss Camp, Western Greenland. Seismic stations are numbered 1-10. Dark patches are melt water lakes and ponds visible during the summer (Google Earth).

Figure 3.2.2 One of the seismic stations deployed (left). The three-component seismic sensor is buried 3 meters below the surface some four meters from the waterproof barrel. Inside the barrel (right) the data logger and voltage regulator sit on insulating foam under which there is the power source, a 12V/100 Ah dry battery. A GPS antenna is attached to the back of the solar panel.

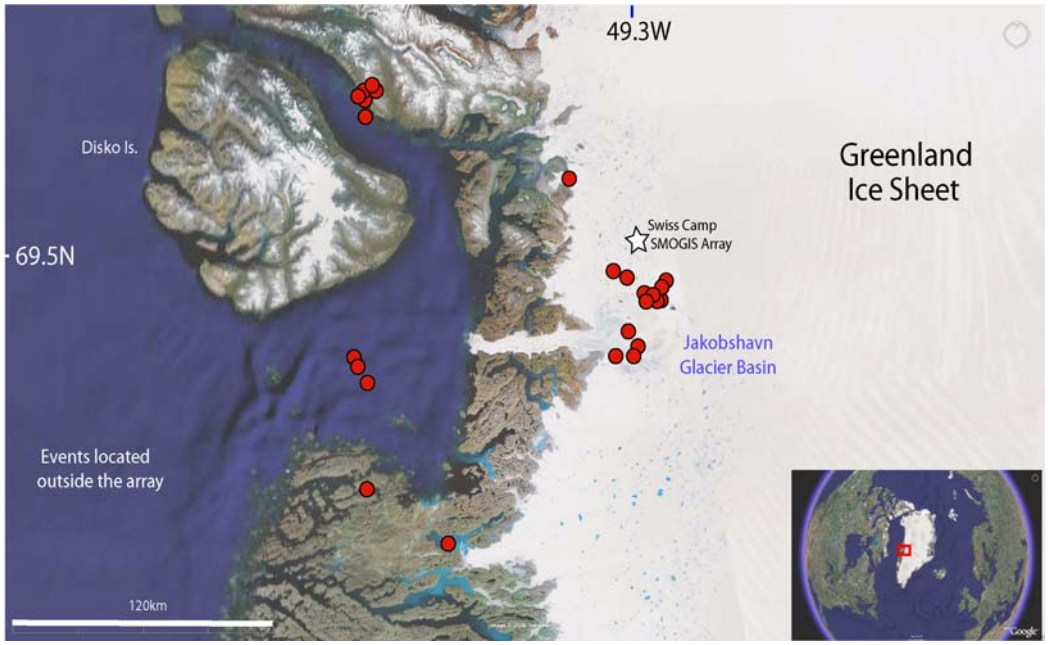

Figure 3.2.3 Seismic events (red filled circles) located during the season May-August 2006 outside of the SMOGIS seismic array. Focal depths are mostly unconstrained but assumed to be no deeper than 30 km. The seismicity to the south of the array, in the Jacobshavn glacier basin, appears to be related to the glacial earthquakes detected with the global seismic network (See Fig 8). Events ~140 km to the west and southwest of the array are classified as tectonic (see Figure 3.2.5).

Ten three-component, continuous digital recording PASSCAL (www.passcal.nmt.edu) seismic sensors were deployed for over three months (May 12-August 15, 2006) at the locations shown in Fig. 3.2.1. Each seismic station was equipped with a three-component L-28 high-frequency sensor (natural frequency 4.5 Hz), a Reftek-130 data logger with capacity for 4GB of data, voltage regulator and dry battery. The battery is constantly recharged by a solar panel. A GPS receiver is attached to the solar panel and provides the coordinates and clock for each station. The battery, data logger and regulator are all housed in a waterproof plastic barrel (Fig. 3.2.2).

3.2.2 Preliminary results of seismic work

Following are the results of the first deployment of the SMOGIS seismic array. Since no prior information existed about the seismicity around Swiss Camp, one important objective of this first deployment was to determine the location, character and spread of seismic activity in the region that will serve to plan the extent and geometry of future deployments. The preliminary results of the survey are shown in Figures 4, 5 and 7. Essentially, three different types of seismic events were detected:

1. Tectonic events, with well-developed P- and S-waves, most located ~140 km to the WNW and WSW of the array (Figs. 3.2.3 and 3.2.4). Estimated local magnitude: 2-3.5.

2. Bedrock events, usually with poorly developed S-waves, likely to occur at the boundary between the ice sheet and the underlying rock, usually located south of the array (Figs. 3.2.3, 3.2.5, 3.2.7a). Estimated local magnitude 2-3.

3. Icequakes, impulsive events, with strong and sharp surface waves, resembling the typical seismogram produced by a single force source in a semi-infinite half-space

(Figs. 3.2.4, 3.2.7b). The estimated local magnitudes are in the range 0-1.

Tectonic events: These events are called 'tectonic' since in contrast to other events in the area their seismograms (Fig. 3.2.5) are consistent with the characteristics of earthquakes produced by double couple, pure-shear sources (*Aki and Richards*, 2002). Their frequency content is relatively high, centered at about 10 Hz.

During the first month of the deployment (mid-May to mid-June) tectonic events occurred with an average frequency of once a day. Beginning June 10th and lasting until June 17th an unexpected increase in the frequency of events occurred (up to 5 events per day). By June 18th the seismic swarm had subsided back to one event per day, staying at that level for the remainder of the deployment. The swarm occurred close to the summer solstice (June 21st), which might suggest seasonal forcing, however, the peak activity happened almost a week earlier, on June 15th.

The tectonic events come from small, seemingly localized areas (S-P interval nearly constant at 20s) some 140 km west and southwest from the SMOGIS array, a region not covered by terrestrial ice. A relation of these events to regional glacial rebound is possible given that, taken all together, their locations roughly parallel the western margin of the GIS (Fig. 3.2.3).

The cause(s) of these events will be investigated fully, as their origin may shed light on the local tectonic regime and the state of stress of the shallow crust, which may in turn reveal a relationship with ice sheet mechanics.

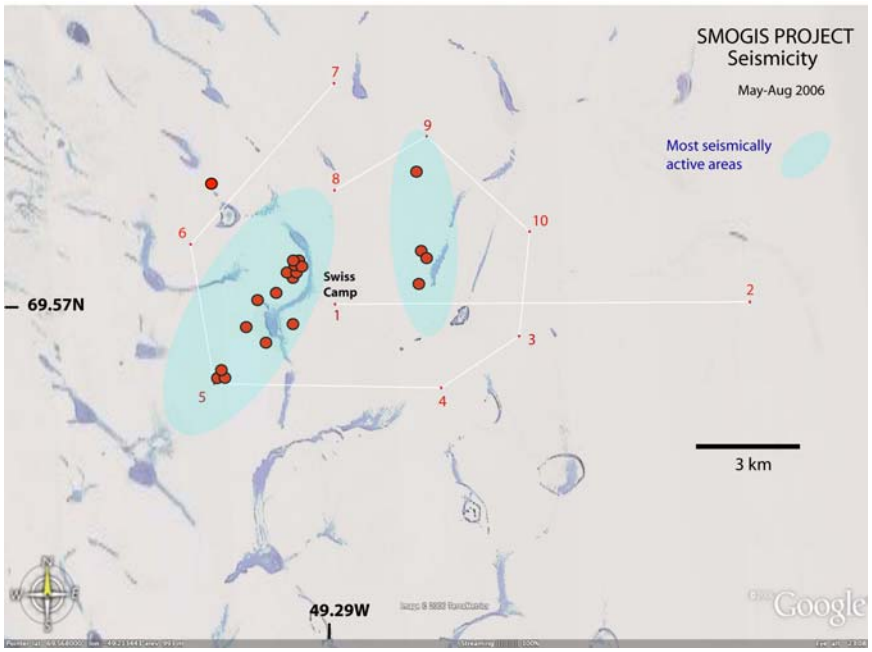

Figure 3.2.4 Preliminary locations of seismic events near and inside the seismic array (Seismic stations are numbered 1 through 10). The colored elliptical areas contain the most seismic activity with many more events than those indicated. Shown event locations can have errors as large as 1 km because a few events are of very low magnitude and recorded in two or three stations only. We shall locate several seismic stations within the ellipses in the 2007 deployment.

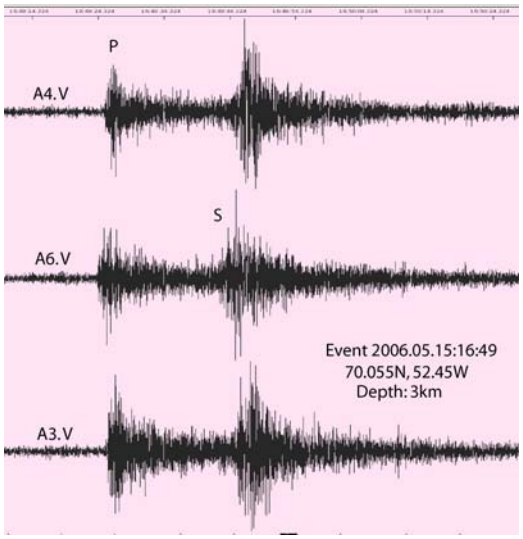

Figure 3.2.5 A tectonic event recorded by stations 4, 6 and 3 (vertical components) in the array show strong S-waves and general signature likely produced by a double-couple mechanism. Most of the tectonic events have similar seismograms as those shown and are ~140 km to the W and WSW of the array (see Figure 4).

Figure 3.2.6 Landsat TM 1990 image of the Jacobshavn glacier basin showing the 'bedrock' events detected in May-August 2006 by the SMOGIS array (red circles), and the epicenters of 'glacial earthquakes' (light green circles) from 1998 to 2005 obtained from teleseismic measurements (Tsai and Ekström, 2006). Compare with Fig. 3.2.3.

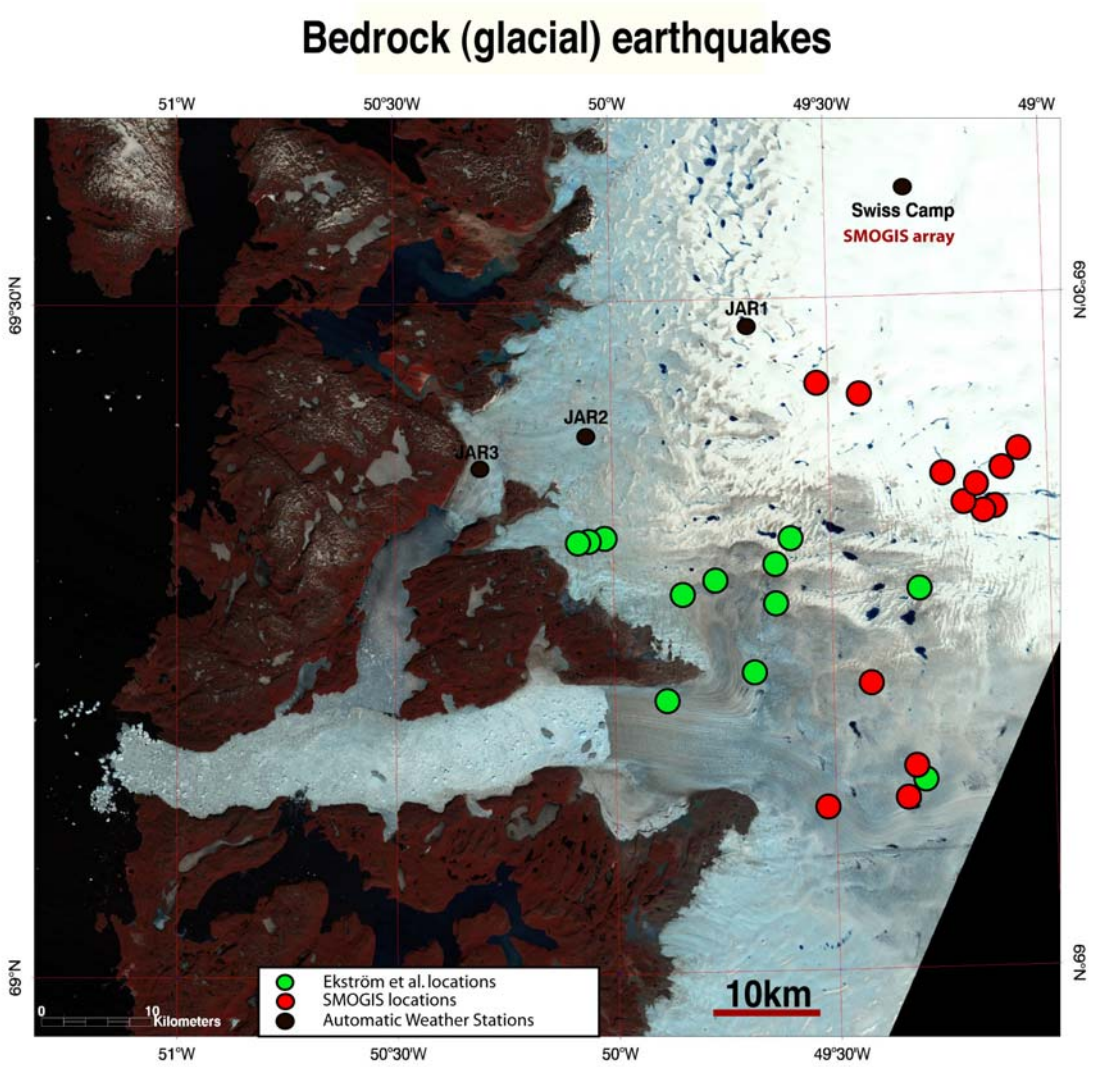

Bedrock events Typically these events show strong P-waves but weak to inexistent S-waves, even in the horizontal components (Fig. 3.2.7a). The predominant frequency is low, usually less than 2 Hz, a fact that contrasts with the tectonic events, which, located much farther from the array have higher frequency content. Fig. 3.2.6 shows that the epicenters of the bedrock events (red filled circles) are located in the Jakobshavn glacier basin, and some are on the ice streams near the glacier outlet, some 60 km south of the SMOGIS array.

These epicenters are in several cases near or coincident with those located by *Tsai and Ekström* (2006) and identified as glacial earthquakes, whose teleseismic signal is predominantly long-period (35-120s). The seismic instruments deployed in SMOGIS are high frequency detectors and do not record such long period signals. Instead, most bedrock events recorded at SMOGIS involve short source time histories, similar to those usually recorded in and near ice stream areas of Antarctica (*Anandakrishnan and Bentley*, 1993; *Danesi et al.*, 2006). Coincidentally however, SMOGIS detected three major events in June and July 2006 with the same origin times and location as detected by *Tsai and Ekström* (2006) using the global network. We shall return to discuss these important events later on (see Fig. 3.2.7 below).

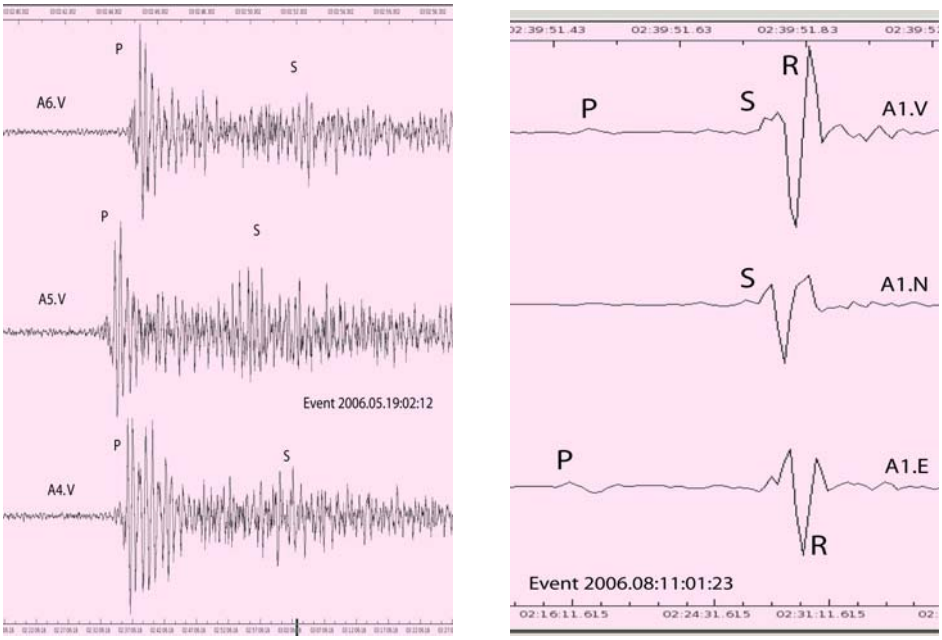

(a) (b)

Figure 3.2.7. (a) Vertical components of a bedrock event at three stations in the array. The predominant frequency is 2Hz and there is little shear wave energy even in the horizontal components. This event is 34km south of the array. Focal depth is unconstrained. (b) A typical simple source icequake 0.9km from station A1 (The S-P interval is 0.3s). The strong Rayleigh wave (R) suggests a shallow source. Events like this are more common as the warming seasons develops and occasionally can be detected in more than three stations. Figure 4 above show epicenters of icequakes most of which have a similar signature to that in the figure.

Icequakes These seismic events are characteristically of small local magnitude (0-1), rarely detected by more than three stations. Most are very shallow as suggested by a strong Rayleigh wave and by the fact that their distance to recording stations is usually less than the thickness of the ice sheet at that locality (Fig. 3.2.7b). The icequakes appear to reflect single force sources, likely opening or expanding crevasses. Work is in progress to reproduce the characteristic seismograms with three dimensional elastic wave solvers. The icequake recording shown in Figure 8b is typical. The seismogram is not only simple but also closely resembles the well-known solu-

tion to the Lamb's problem in elastodynamics (e.g., *Lamb*, 1904; *Fung*, 1965) for a point force acting on the surface of an elastic, isotropic, solid and homogeneous half-space. Since the ice sheet is probably neither homogeneous nor isotropic the source-receiver seismic rays for these events must not penetrate much into the ice, which is consistent with a shallow source.

Other recorded events. In addition to the types mentioned above the SMOGIS array recorded a number of high frequency, undifferentiated events, likely seismic signals produced by calving of the ice at the glacier terminus. Most of these events are long wave trains with no distinguishable P or S wave arrivals although some show amplitude modulation. The frequency spectrum is usually centered at about 5 Hz.

SMOGIS also recorded near-field events that appear to be related to the fracturing of large crevasses. At the end of the deployment it was discovered that station 5 had been unwittingly installed on the packed snow covering a large vertical crevasse oriented NNE. Records from the station show continuous icequake activity with zero or near zero S-P time intervals accompanied by later arrivals with similar waveforms of smaller amplitude, apparently waves reflected from the ends of the crevasse.

In summary, the SMOGIS seismic deployment has successfully detected a substantial number of seismic events which provide useful clues as to where best explore the dynamic response of the ice sheet in the peripheral region, what sort of information is possible to obtain with seismic sensors, and how and where to link these with local and satellite measurements of ice motions. We expect to have more significant results after the 2007 deployment.

3.3 Geodetic Program

3.3.1 Local GPS measurements in Ilulissat

A glaciological geodetic program was maintained since 1991 to determine flow velocity, deformation, and elevation change of the inland ice in the western part of the Greenland ice sheet. The measurements were carried out by 3 members of Stuttgart University of Applied Sciences between August 10th and August 24th, 2006.

There are two main test areas. The first test field at Swiss-Camp (ETH/CU-Camp) was started in 1991. It consists of 4 stakes (triangle with 1 point in its centre). A total of 9 field campaigns were carried out in this test field. The second test field was established in 2004. It has the same design than at Swiss Camp (4 stakes, triangle with 1 point in its centre). ST2 is situated at 69° 30' 28" N; 49° 39' 09" W, ellipsoidal height = 1000 m, hence 170 m lower than Swiss-Camp, approximately 14 km south-west from Swiss-Camp and approximately 1,5 km up-glacier from JAR1. Here we have now three campaigns in 2004, 2005 and 2006.

The measuring program 2006 was similar to previous campaigns. All GPS measurements were done by 2 receivers Leica System 500 and 2 receivers Leica System 1200, with real-time equipment.

- GPS reference point EUREF 0112 in Ilulissat on solid rock,
- Long-time GPS measurement at point YOUTH HOSTEL in order to investigate GPS multi-path effects and ionosphere interferences of GPS-signals.

ST-2 (August 15th, 2006)

- Static GPS baseline 65 km to EUREF 0112 in Ilulissat, measured for 8 hours,
- Temporal ice GPS reference on central stake ST200,
- Measurement of the actual positions of all 4 stakes ST200, ST201, ST202 and ST203,
- Topographical survey of ice surface (no snow cover left) by grid points every 200 meters and kinematics GPS profiling, area 1.6 x 1.6 km^2.

Swiss-Camp (August 17th, 2006)

- Static GPS baseline 80 km to EUREF 0112 in Ilulissat, measured for 7 hours,
- Temporal ice GPS reference (point 106.1) at Swiss-Camp for real-time GPS around Camp area,
- Measurement of the actual position of point 106.1 near the Camp. The other stakes of the deformation network were melted out and could not be measured. Two old wooden central sticks (from 1991) were found and were measured instead of the lost alu-stakes.
- Reconstruction and staking out of old positions from 1994, 95, 96, 99, 2002, 2004 and 2005.
- Measuring actual heights at all these old positions by real-time GPS,
- Measuring of snow depth in order to reduce heights to ice surface,
- Topographical survey of snow surface around Swiss-Camp by grid points every 200 meters and kinematics GPS profiling.

3.3.2 Results

Swiss Camp Area: The measurements in 2006 had been carried out on August 17th, with an air temperature of +1°C. The surface was very wet with a lot of superficial water. The remaining snow layer was about 0.2 – 0.3 m. All measurements were reduced to the ice horizon. All heights are absolute heights (reference point EUREF 0112 in Ilulissat on solid rock).

Elevation changes can be derived from the ice surface topography as well as from concrete previous point positions. Both methods result in the same average elevation change. Fig. 3.3.1 shows the elevation change from concrete (previous) stake point positions.

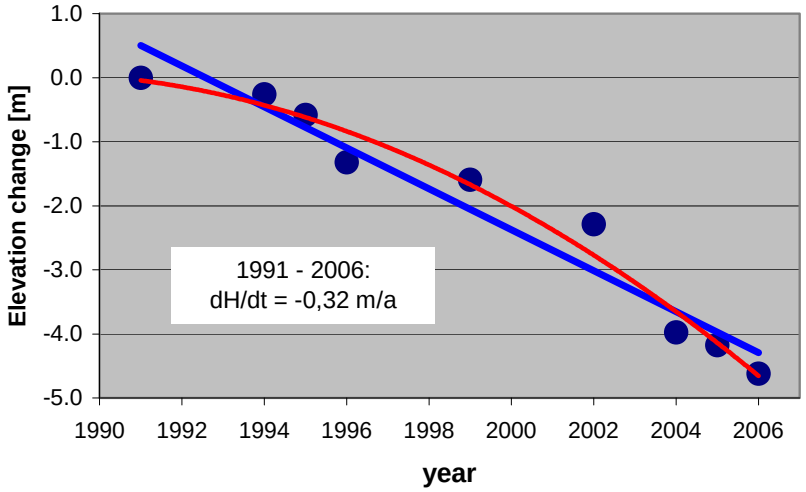

Figure 3.3.1 Swiss Camp: Elevation change of ice horizon 1991 – 2005

The adjusted straight line over the whole period 1991 - 2006 shows an average elevation change of –0.32 m/a. Temporal variations up to a decrease of –0.85 m/a according to higher summer air temperature are clearly visible. All the extremely big elevation changes 1995-1996, 2002-2004

and also 2005-2006 coincide with the highest summer air temperatures. In the last year we find an elevation decrease of –0.44 m per year. In the years 1991 until 2002 the linear trend was –0.22 m/a.

The terrain around Swiss-Camp has a smooth topography with uniform terrain inclination. The elevation change, derived from digital terrain models differences in 2005 and 2006 (Fig. 3.3.2) shows little irregular values, mostly agreeing with the average –0.4 m/a from the stake positions.

The ice flow vector was determined by comparison of stake positions in different years. As mentioned before, only one aluminum stake (106.1, near Swiss Camp) was still upright, all others were melted out and were fallen down. From two points, old wooden sticks were found, which formerly had been planted one meter next to the aluminum stake and can now be used for displacement measurements.

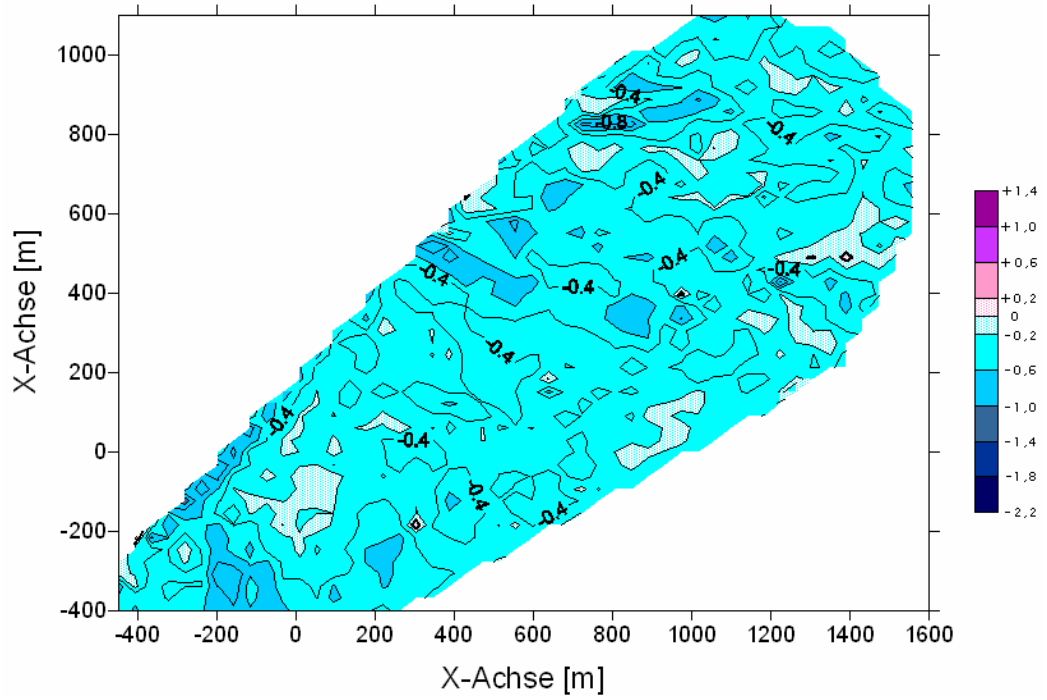

Figure 3.3.2 Elevation change [m/a] at Swiss-Camp from difference digital terrain models 2006 – 2005. Local coordinate system (origin Swiss Camp 1999).

The resulting ice flow velocity in average is 0.317 m/d. With one exception, 1995-1996, we find continuously increasing values with years (Fig. 3.3.3), probably due to more melt water at the bottom with increased sliding on the bedrock (*Zwally et al.*, 2002)

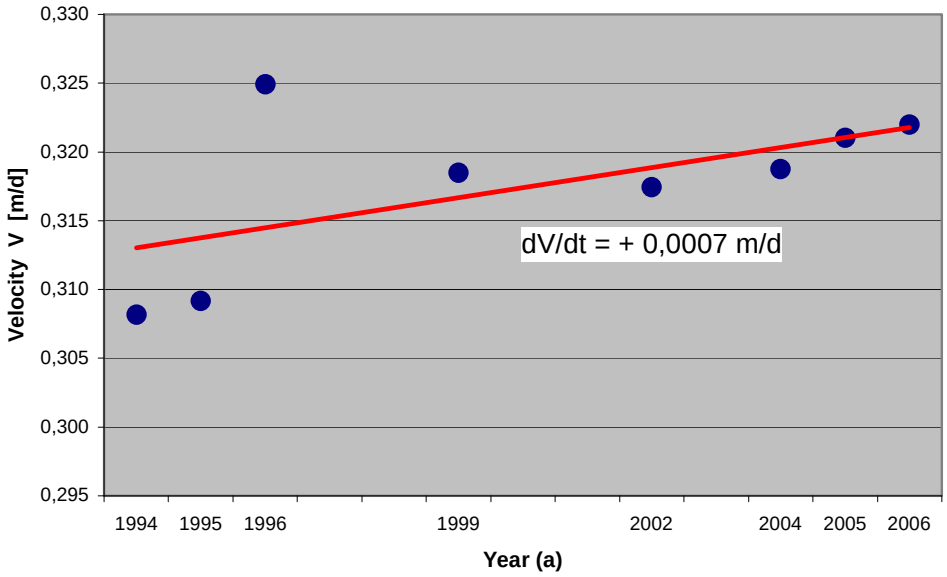

Figure 3.3.3 Swiss Camp: Ice flow velocity [m/d], 1991 – 2006

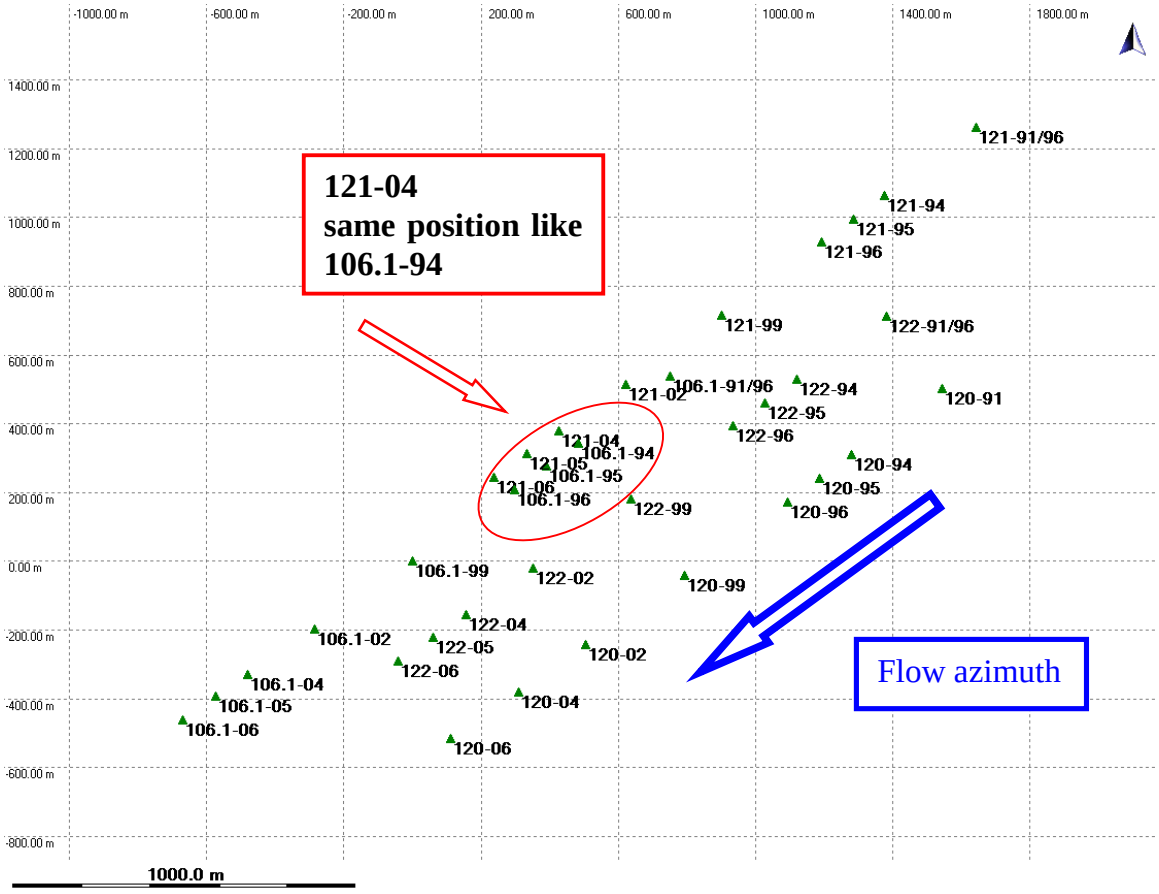

Figure 3.3.4 Swiss Camp: Stake positions in different years, 1991 – 2006

During 15 years (between 1991 and 2006) all stakes had moved downstream by 1.75 km. It is possible that the flow velocity is varying with local position, and not only with time. In order to examine the local influence on velocity, we compared velocities of stakes in similar positions, but different years (Fig. 3.3.4). For this purpose the stakes in the network were placed such that 2 stakes (121 and 106.1) were situated almost exactly in the flow direction (mean azimuth = 260.6 gon). A comparison after 10 years (Tab. 3.3.1) shows a significant increasing of flow velocity at the same position! The flow azimuth is still constant.

Table .3.3.1 Comparison of ice flow velocity at same position after 10 years

Point	Period	Flow velocity [m/d]	Flow azimuth [gon]
106.1	19.06.94-26.06.95	0.309	260.547
121	14.08.04-04.08.05	0.318	260.713

In summary, our results indicate that elevation change (net surface lowering by melting) continuous since 1991, with some extremely high rates during warm summers. This is in agreeing with the overall observed global warming, and in particular increasing air temperatures in Polar Regions**.**

ST2 Area: The area "ST2" is situated at 1000m altitude, 150 m lower than "Swiss Camp". This test field was established in 2004 and re-measured first time in 2005 and now again in 2006. At the time of the measurement (August 15th , 2006) the surface was hard and without melt water; there was no snow cover left on the ice surface. All measurements were directly referred to the ice horizon.

The elevation change was derived from digital terrain model (1.6 x 1.6 km^2 area, 2004, 2005 and 2006) using grid points every 200 meters, and some kinematics GPS profiles. On average we found an elevation decrease of -0.38 m/a between 2004 and 2005, and for the 2005-2006 period, a decrease of –0.30 m/a was observed. Both periods are too short for a long term interpretation. The average linear trend of –0.34 m/a is close to the value found for the Swiss Camp region. The stakes are still anchored 1.5 – 2 meters in the ice and can be used for further measurements.

The ice flow vector of area "ST2" as average from all 4 stakes is shown in Tables 3.3.2 and 3.3.3. Flow velocity and flow direction (azimuth) are significantly varying from point to point. Especially point ST201, situated in the Eastern part, differs in velocity and azimuth from those of most other stakes, probably due to specific topography at surface and bedrock.

In average the flow velocity is 0.20 m/d with a flow azimuth 266.4 gon.

Table 3.3.2 Ice flow velocity in all campaigns at ST2

Period	2004-2005 m/d	2005-2006 m/d	2004-2006 m/d
Average of flow velocity	0.200	0.197	0.198
Standard deviation, one point	0.006	0.006	0.007
Standard deviation, average 4 points	0.003	0.003	0.004

Table 3.3.3 Ice flow azimuth in all campaigns at ST2

Period	2004-2005 [gon]	2005-2006 [gon]	2004-2006 [gon]
Average of flow azimuth	266.016	266.403	266.209
Standard deviation, one point	3.325	3.346	4.056
Standard deviation, average 4 points	1.662	1.673	2.342

Deformation and strain at ST2 can be calculated from distortions in the stake network between 3 campaigns (2004, 2005 and 2006). Method and formulas are described in *Welsch* 1982.

Interesting parameters are:

e_1 = principal strain rate in main deformation azimuth Θ (principal axis of strain ellipse),

e_2 = principal strain rate in main deformation azimuth Θ + 100 gon.

Using the incompressibility condition, the vertical component e_3 is calculated from $e_3 = -(e_1 + e_2)$. The numerical results are given in Tab. 3.3.4, and graphically in Fig. 3.3.5 as example for the longest period 2004 – 2006.

Table 3.3.4 Strain rates at ST2

Epochs	Points	Azimuth Θ of e_1 [gon]	horizontal strain rates e_1 [ppm/a]	e_2 [ppm/a]
2005→2004	ABCD	370.3	8548	-1951
	ABC	370.3	8552	-1953
2006→2005	ABCD	369.8	8295	-2508
	ABC	369.8	8298	-2511
2006→2004	ABCD	370.0	8445	-2243
	ABC	370.0	8449	-2245

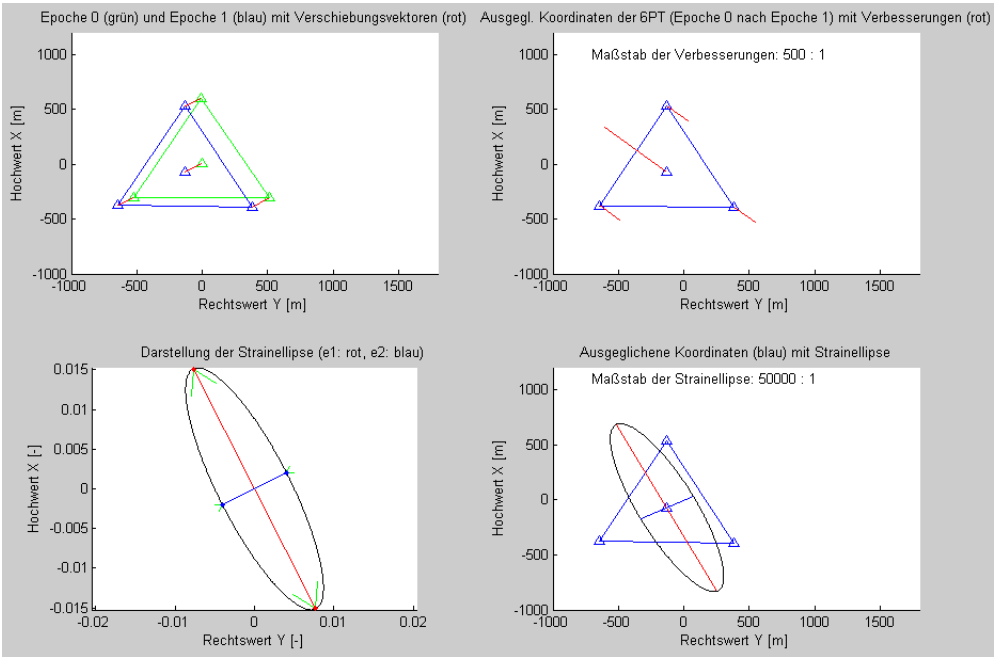

Figure 3.3.5 Graphic display of strain-analysis in test field ST2, 2004 – 2006

The main distortion is almost perpendicular to the flow direction in ST2 (260.6 gon), due to differing horizontal flow directions of the 4 stakes which cause a spreading of the ice surface across the flow line. The incompressibility condition would lead to e_3 =-6202 ppm/a, and if we suppose the ice thickness (H) at ST2 of approximately 500 m, we obtain an ice thickness change by outflow of $\Delta H = e_3 * H$ = -3.1 m/a. As we find a real elevation change of the ice surface of only -0.34 m/a (negative mass balance), most of the out flowing ice is replaced by snow accumulation and conversion into new ice.

3.3.3 Surface and bedrock topography

As an overview we show the Landsat image of the Ilulissat area, together with our results of the ice flow vectors (Fig. 3.3.6. The general direction of the ice flow is towards the Ilulissat glacier, which is draining about 6% of the Greenland ice sheet.

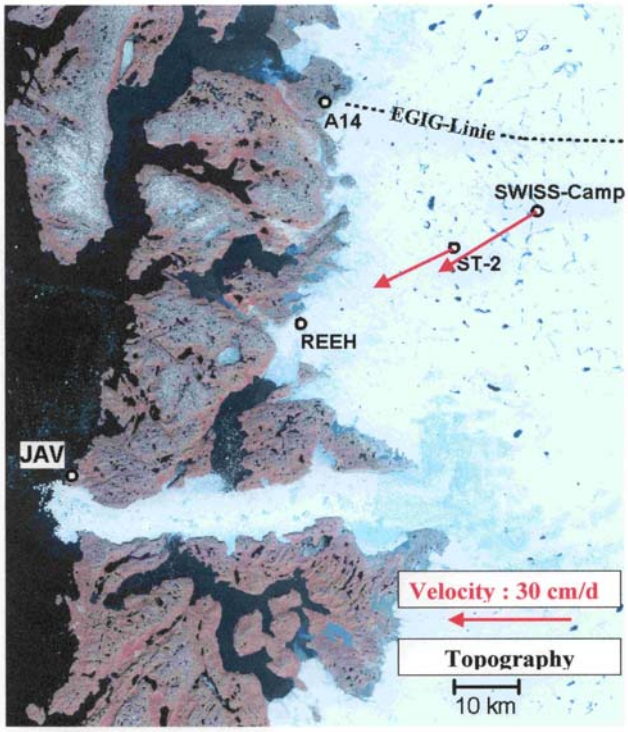

Figure 3.3.6 Research areas and ice flow vectors (Landsat image, July 7th, 2001)

Distinguishing features in both test areas, “Swiss Camp” and “ST2”, are:

- altitude above ellipsoid WGS84 (Swiss Camp = 1170 m, ST2 = 1000 m),
- distance from ice margin (Swiss Camp = 28 km, ST2 = 16 km),
- surface topography (Swiss Camp less inclination, more smooth),
- meteorological conditions (air temperature, precipitation)
- ice thickness
- bedrock topography

The components surface topography and bedrock topography will be discussed here. For this study we use the data kindly received from *Steinhage* 2006. Origin and quality of that data is unknown and might be influenced by some artifacts in some cases.

The bedrock topography (Fig. 3.3.7 and 3.3.8) appears very irregular. Some parts, especially close to ST2 and east of Ilulissat glacier basin, are dominated by high mountains, which would interfere ice flow. These high mountains would also cause reduced ice thickness in some parts (Fig. 3.3.9). The ice thickness at ST2 is only about 500 meters based on Fig. 3.3.9, and about 1100 m at Swiss Camp.

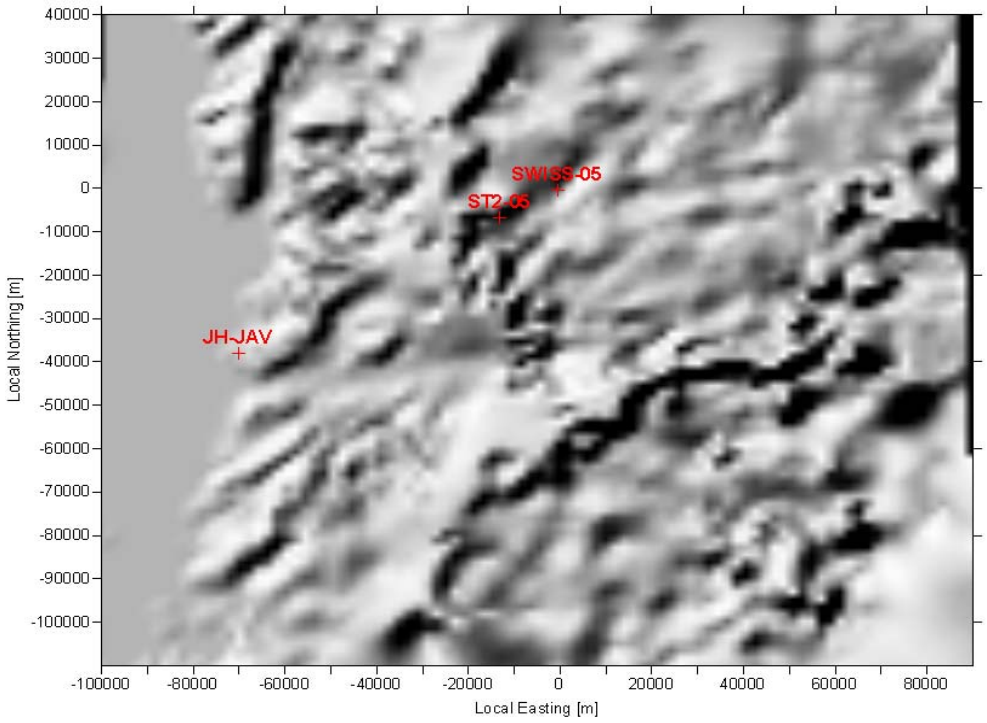

Figure 3.3.7 Bedrock topography in the Ilulissat area.

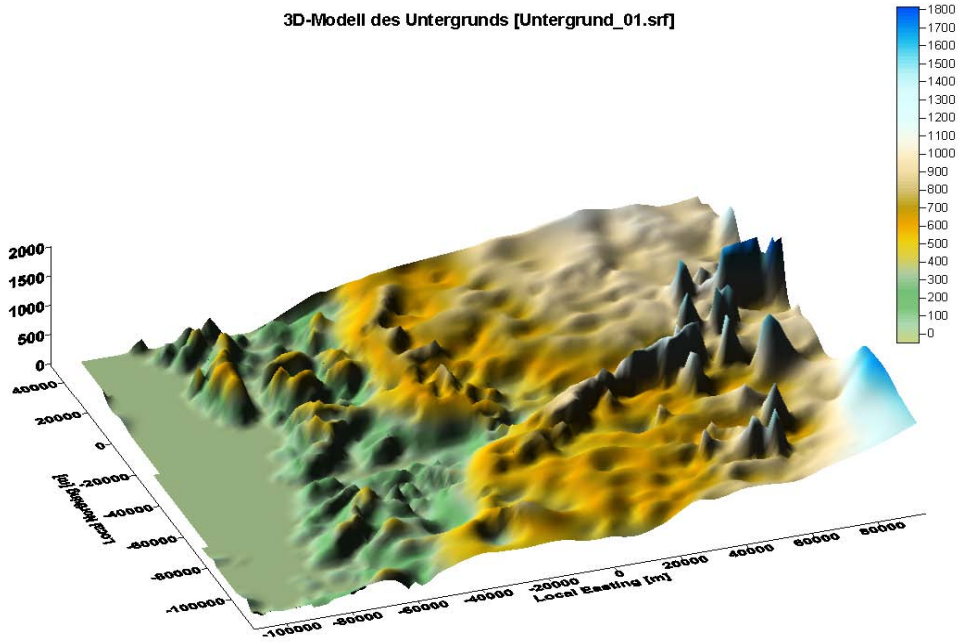

Figure 3.3.8 Bedrock topography in the Ilulissat area, 3D-visualization

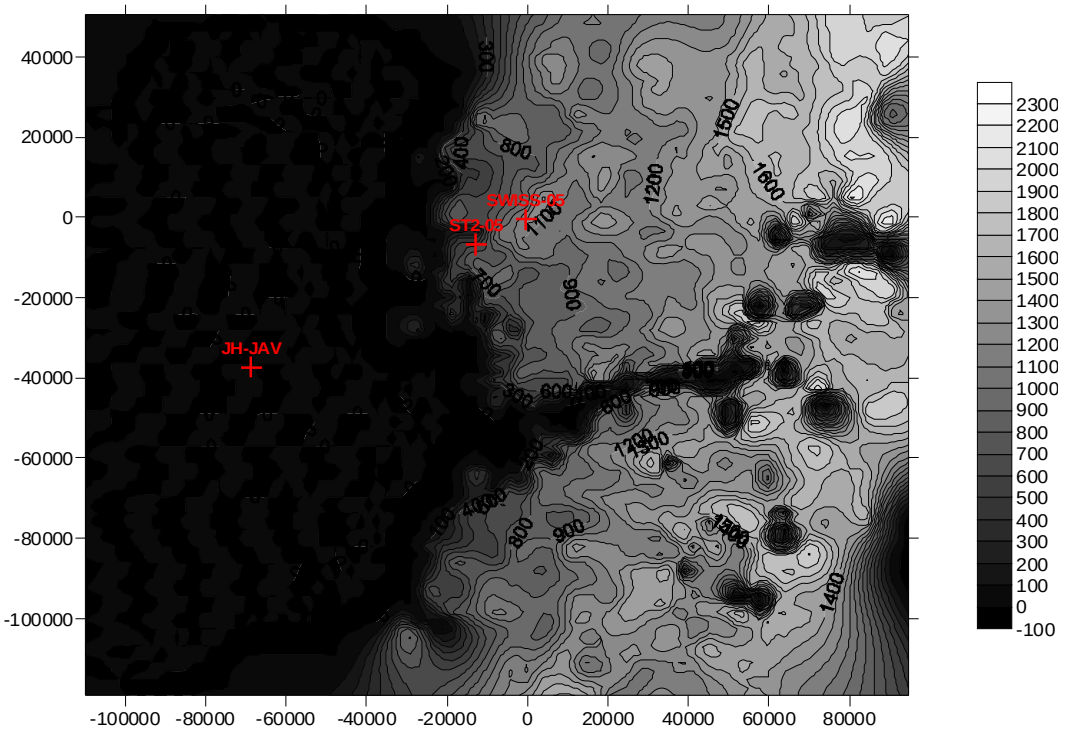

Figure 3.3.9 Ice thickness in the Ilulissat area, contour lines (interval = 100 m)

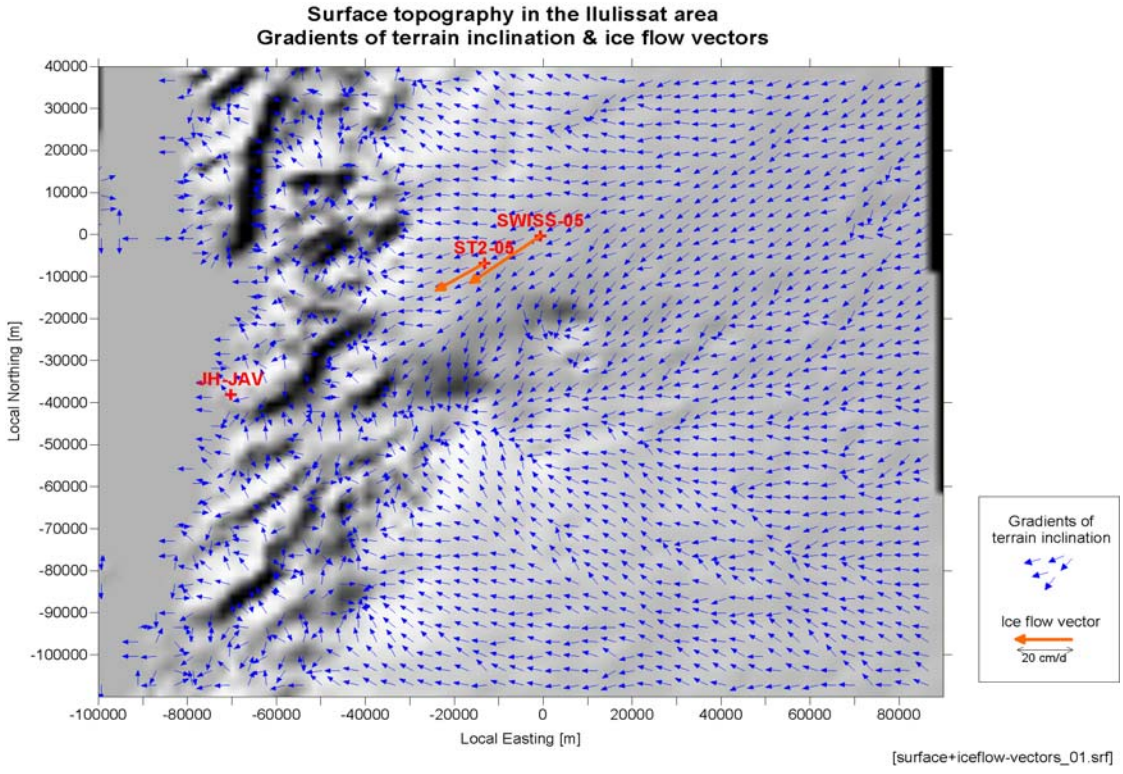

Figure 3.3.10 Surface topography in the Ilulissat area with gradients of terrain inclination, and ice flow vectors at Swiss-Camp and ST2.

The ice surface topography with gradients of maximum terrain inclination and ice flow vectors is shown in Fig. 3.3.10. At Swiss Camp, the surface and rock bottom is less disturbed, and hence the flow velocity is greater than at ST2. The flow direction is mostly correlated with gradient of big scale topographic inclination.

3.3.4 Summary

The investigation of temporal and spatial variation of mass budget parameters was obtained in the new test field ST2 since 2004. The results of both test areas (Tab. 3.3.5, Fig. 3.3.10) show about the same elevation decrease of –0.3 m/a for the time period 2004-2006; hence, the surface was lowered, the mass budget is negative. It demonstrates the high sensitivity of increasing air temperature, especially in the ablation area near the ice margin.

Table 3.3.5 Summary: Elevation change and flow vectors at Swiss-Camp and ST2

	Swiss-Camp (ell. altitude = 1170 m)			**ST2 (ell. altitude = 1000 m)**		
	2004 - 2005	**2005 - 2006**	**Trend 1991-2006**	**2004 - 2005**	**2005 - 2006**	**Trend 2004-2006**
Elevation change [m/a]	-0.20	-0.44	-0.32	-0.38	-0.30	-0.34
Flow velocity [m/d]	0.322	0.324	0.318	0.200	0197	0.198
Flow azimuth [gon]	261.468	260.983	260.787	266.016	266.403	266.209

4. Proposed Field Activities and Research Objectives 2005

4.1 AWS Maintenance

The automatic weather station network will be maintained. In the north, the Petermann ELA stations will be serviced as part of the NSF/NASA supported field activities. We will visit the new NEEM AWS to download the data for the new deeps ice core camp. Further, GITS and NASA-U along in the north-western part of the ice sheet, as well as the AWS sites NGRIP and Summit in the dry-snow region will be serviced. The profile JAR2, JAR1, CU/ETH, and Crawford 1 will be serviced while at the Swiss Camp. In the southern part of the ice sheet we will service the DYE-2, Saddle, NASA SE, and Saddle (Fig. 1.1) to reactivate the satellite transmitter, download the data and collect snow stratigraphy information.

4.2 GPS Network Maintenance

Our effort to monitor the ablation along a transect from the Swiss Camp to the ice margin will continue. We will service the GPS network in collaboration with Dr. Jay Zwally (NASA-GSFC) and will add two new GPS monitoring stations in the Jakobshavn region. We will continue to collect high-resolution surface topography data using Trimble Pathfinder differential GPS measurements along several transects in the lower ablation region. In addition, we will acquire a sequence Landsat TM satellite imagery during the onset of melt and melt period to monitor the spatial variation and extent of snow fields in the ablation region.

4.3 Ground Penetration Radar

We have collected a number of ground penetrating radar (GPR) profiles along the western slope of the ice sheet (Jakobshavn and Kangerlussuaq region) in previous field seasons (1999, 2000, 2003). The analysis of this data set showed that the accumulation could vary up to 40% between the trough and the ridge of the undulation. The surface topography with scale length of several kilometers plays an important role for the spatial variability of accumulation, the mass transfer, and the surface energy balance. We will repeat some of these GPR measurements during the spring 2007 field season along the same profiles to verify the recent accumulation changes and high percolation events in that region.

4.4 Seismic Monitoring

In spring 2008 (later April and May) we will install ten seismic receivers in areas of seismic activity based on the 2007 data. A semi-permanent base station will be installed at the Swiss Camp, and two stations on bedrock to the north and south of the Jacobshavn glacier ice front. In sprint 2009 (late April and May) we will install additional stations around centers of seismic activity and maintain the 10 stations installed in the previous year.

5. References

Abdalati, W. and K. Steffen. Greenland ice sheet melt extent: 1979-1999, *J. Geophys. Res.*, 106(D24), 33,983-33,989, 2001.

Aki, K. and P. Richards. *Quantitative Seismology*, 2d Ed., Univ. Science Books, 2002.

Anandakrishnan, S. and C.R. Bentley. Micro-earthquakes beneath ice streams B and C, West Antarctica: Observations and implications, *J. Glaciol.*, **39**, 455-462, 1993.

Box, J.E. and K. Steffen. Sublimation on the Greenland ice sheet from automated weather station observations, *J. Geophys. Res.*, *106*(D24), 33,965-33,982, 2001.

Box, J.E., D.H. Bromwich, B.A. Veenhuis, L-S Bai, J.C. Stroeve, J.C. Rogers, K. Steffen, T. Haran, S-H Wang. Greenland Ice Sheet Surface Mass Balance Variability (1988-2004) from Calibrated Polar MM5 Output, *J. Climate*, 19 (12), 2783-2800, 2006.

Danesi, S. et al. Repeating earthquakes from rupture of an asperity under an Antarctic outlet glacier, *Earth and Planet. Sc. Lett.* (in press, available online), 2006.

Lamb, H. On the propagation of tremors over the surface of an elastic solid. *Phil. Trans. Roy. Soc.* (London) Ser. A, 203, 1-42, 1904.

Fung, Y.C. *Foundations of Solid Mechanics*, Prentice-Hall Inc., New Jersey, 1965.

Nghiem, S. V., K. Steffen, R. Kwok, and W.Y. Tsai. Detection of snow melt regions on the Greenland ice sheet using diurnal backscatter change, *J. Glac.*, *47*(159), 539-547, 2001.

Nghiem, S. V., K. Steffen, G. Neumann, an R. Huff. Mapping of ice layer extent and snow accumulation in the percolation zone of the Greenland ice sheet, *J. Geophys. Res.*, *110*, F03017, doi:10.1029/ 2004JF000234, 2005.

Shuman, C., K. Steffen, J. Box, and C. Stearn, A dozen years of temperature observations at the Summit: Central Greenland automatic weather stations 1987-1999, *J. Appl. Meteorol.*, *40*(4),741-752, 2001.

Steffen, K., and J.E. Box. Surface climatology of the Greenland ice sheet: Greenland climate network 1995-1999, *J. Geophys. Res.*, 106(D24), 33,951-33,964, 2001.

Steinhage, D. Digital data from ice surface, ice thickness and bedrock, Personal communication, Alfred-Wegener-Institut Bremerhaven, 2006.

Tsai, V and G. Ekström. Analysis of Glacial Earthquakes. Accepted, 2006.

Welsch, W. Description of homogenous horizontal strains and some remarks to their analysis. Deutsche Geodätische Kommission, Reihe B, Nr. 258/V, p. 188-205, München 1982.

Zwally, H.J. W. Abdalati, T. Herring, K. Larsen, J. Saba, and K. Steffen. Surface melt-induced acceleration of Greenland ice-sheet flow, *Science*, 297, 218-222, 2002.